WISE IOC Distortion Calibration

Document number: WSDC D-T033

1. Overview

The WISE optical distortion model is a 4th-order polynomial for each axis, X and Y, plus a skew factor applied to Y. Currently the skew factor is constrained to be zero and is not computed by the calibration program, leaving two 15×15 linear systems of equations to be solved. Details may be found in the gnDSTR SDS, WSDC D-D013.

The data used to calibrate distortion are pairs of associated WISE and 2MASS point sources. These associations are generated as a by-product of the PRex module SFPRex (see the PRex SDS, WSDC D-D003) and are called RvB (Reference vs. Band-frame) files. The positions are in band-frame pixel units, with the 2MASS sky positions mapped, using the final SFPRex band-frame solutions, to band-frame coordinates without any adjustments for distortion. Thus the reference star positions in the RvB are as they would appear in a distortion-free optical system. The WISE positions used by gnDSTR in the RvB files are not corrected for distortion.. The offsets between these pair members are fit to the 4th-order polynomials via chi-square minimization.

Before flight data were available, a Code V ray-trace model for W1 was provided by SDL and used by H. McCallon to generate a pseudo-RvB file. Three scan-mirror positions were included, each sampled uniformly with a 31×31 set of rays. In addition, the simulation data used for WSDC development included distortion, a cubic polynomial model identical in all bands and with corresponding SIP coefficients in all FITS headers. While both of these exercises demonstrated correct execution of the gnDSTR software, adequacy of the 4th-order polynomial, and sample size needed to make model error negligible, neither presented any challenge to the acquisition of a large highly reliable set of RvB data for each band, and that proved to be the driver in IOC.

The Code V model was primarily of interest as an indication of qualitative features to be expected. It did not include any post-beamsplitter optics, and whether the real distortion would vary significantly with band was not known and was not ruled out. Also, the format of the Code V data, being completely different from RvB data, left the orientation ambiguous, and the assumption that all bands would be rotationally aligned was not allowed anyway. This was not a concern, since only qualitative features were of interest at the time, and in fact the vector-flow diagrams used for visualization included all coefficients of the model, unlike the later practice of suppressing the constant terms (for display purposes, that is; all terms are always used for distortion *correction*). Including those terms results in large central distortion vectors and a general appearance that was substantially different from later visualizations of the real distortion, which omitted them. The result was a delay in recognizing that a rotated version of the Code V model did actually have noticeable

similarities to the real distortion.

In IOC, with significant distortion and initially only coarse guesses at its true properties, acquiring pairs of WISE/2MASS point sources in large numbers and with high reliability over entire arrays was nontrivial, especially in the longer wavelengths. Interdependency between band-to-band offsets, scales, and distortion in each band proved greater than expected. An iterative procedure was adopted which allowed the greater distortion in the corners of the arrays gradually to be brought into focus.

The initial plan was to drop the polynomial coefficients below second order generated by gnDSTR before passing the polynomial description into the FITS headers as SIP coefficients. The reasoning behind this was that these terms are already fitted as part of the SFPRex band-frame solutions and could be absorbed into the CD matrix. Although this would have resulted in a clean separation, it turned out not to be practical. That is, it did not achieve the desired accuracy. By allowing the linear terms to remain in the distortion coefficients used, subtle couplings which would otherwise be lost are retained. This does not result in a conflict with the linear terms generated by SFPRex on a frame basis, because the distortion adjustments to WISE positions in band-frame coordinate are made in SFPRex prior to the frame fit.

In QA mode, SFPRex continues to compute all the linear terms as part of its solution for each frameset. Then adjustments to those terms are included via the distortion coefficients in addition to all the non-linear terms. In the 3-parameter mode, which feeds the downstream pipeline, only X and Y translations, along with rotation for band 1, are computed via the SFPRex fit. The other three band-frame positions are computed using *a priori* knowledge gained from the IOC astrometric calibration. As with QA mode, all the linear and nonlinear terms of the distortion coefficients are used. With this hybrid approach, the mission requirements are met.

2. Initial Results

WISE in-orbit checkout began with the Code V distortion model in place for all bands. In retrospect, the initial difficulty finding RvB matches might have been overcome quickly by experimenting with different rotations of the Code V model, since it eventually turned out that the successful distortion models in the four bands all bear a strong resemblance to the Code V model when it is rotated through 270 degrees. In fact, employing it with the face-value orientation must have made finding RvB matches more difficult than if no distortion model had been used. As it happened, the SFPRex module had great difficulty finding matches in the corners. A typical example of the early array coverage by RvB pairs is shown for each band below.

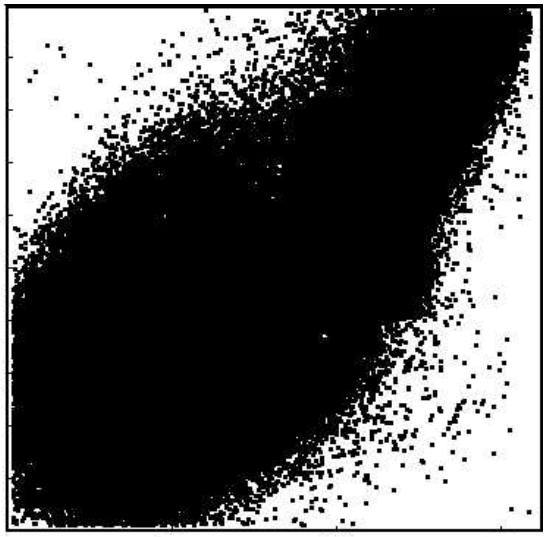

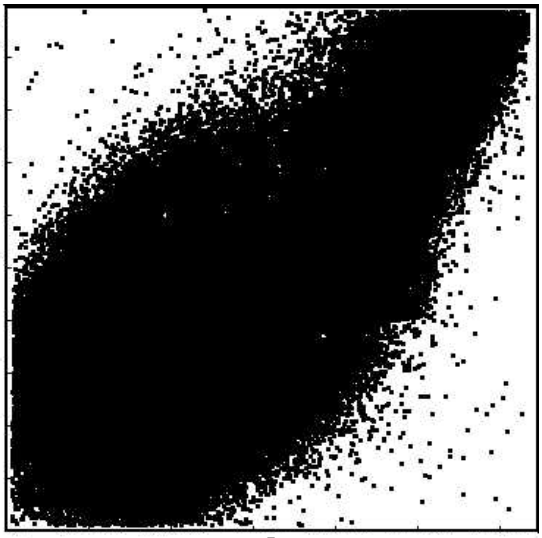

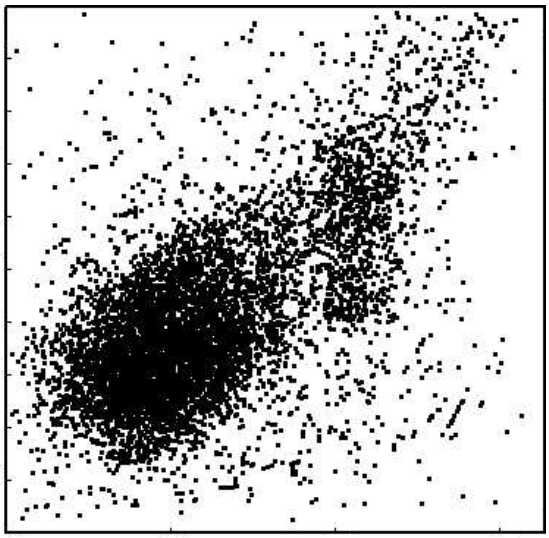

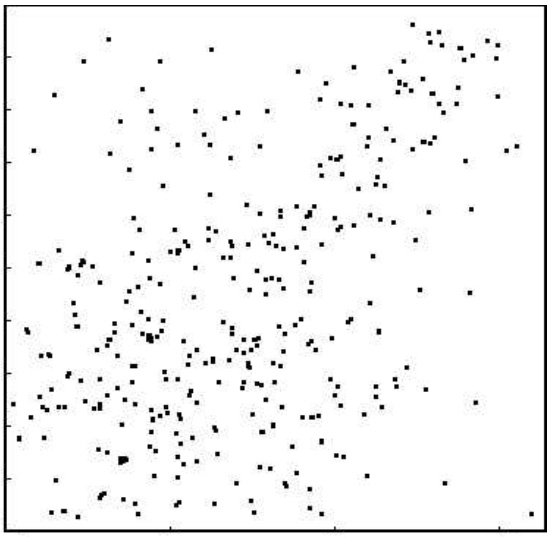

The attempt to acquire more uniform coverage required accepting more questionable matches between WISE and 2MASS sources. This allowed some false matches into the fit, which aggravated the problem. Fortunately, the majority of RvB pairs were legitimate matches, so that the fitting tended in the right direction, but iteration was necessary, and outlier rejection was important. A typical plot of fit residual for each W1 RvB pair is shown below as a function of point number in the sample; the red points are X residuals, the blue points are Y residuals, and the ordinate units are pixels.

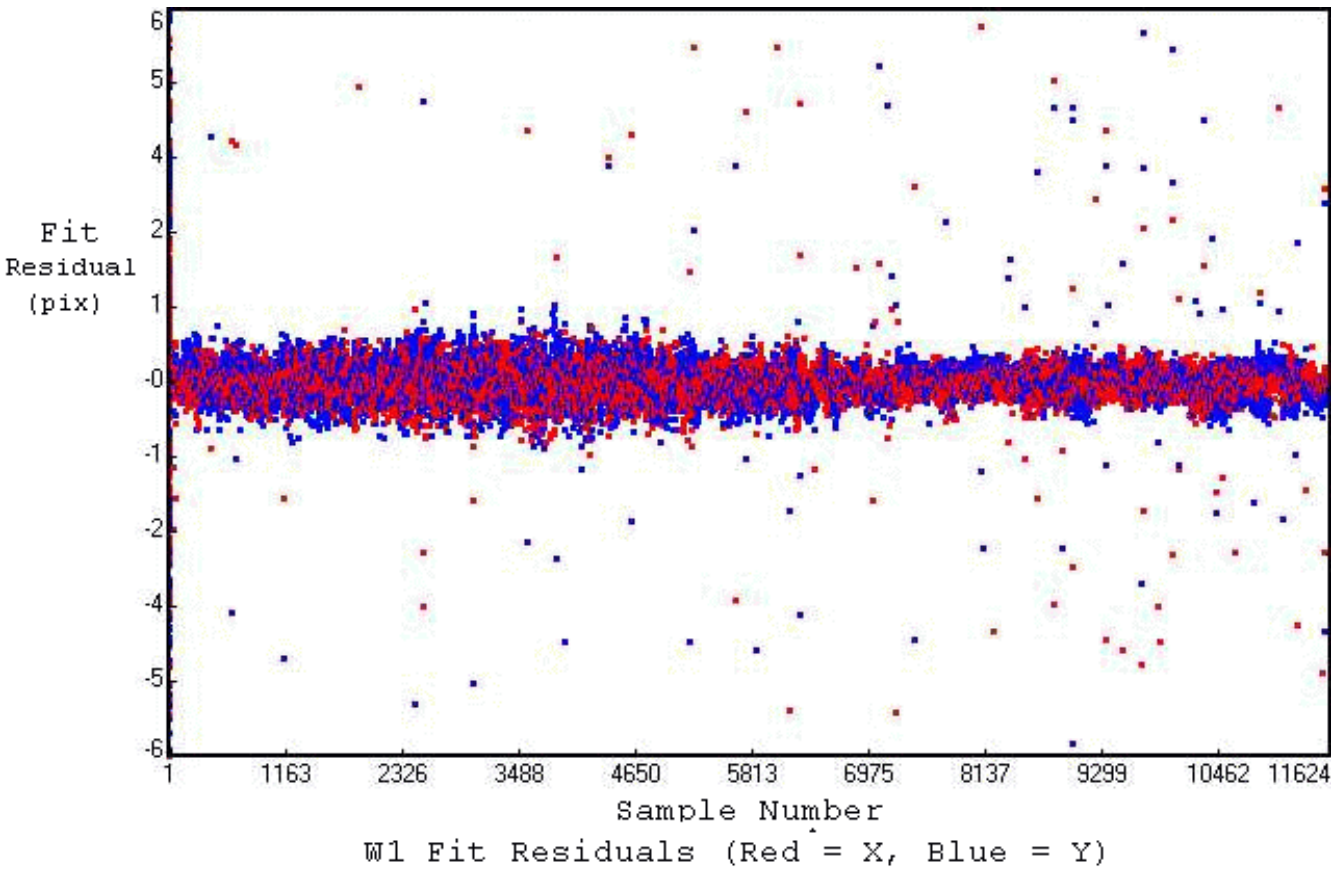

The outlier population is clearly distinguishable from the true RvB matches. This information led to improved outlier rejection in the fitting process.

3. Modifications to the Processing

Modifications were made to the PRex code that collects RvB pairs and to the gnDSTR code that uses the RvB pairs to fit the distortion polynomial. Special implementations of this and other PRex logic were implemented by H. McCallon for streamlined offline analysis. Once it became clear that including a skew term was not helping, it was deleted, and this decoupled the fitting of the two axes. This in turn allowed FITS images of the binned RvB offsets to be fit as ordinary surfaces by the offline program surfit, whose code is completely general in polynomial order. Images of X and Y offsets between RvB pairs were generated by binning at various spatial resolutions, and these were fit to polynomials of order 3 through 9. Third order was seen to be just inadequate, but fourth order left residuals as small as any of the higher orders. It was decided that fourth order was acceptable.

Changes made to the PRex code were as follows.

1.) The PRex internal band-merging criteria were made functionally dependent on radial distance from the center of the array. This allowed tighter criteria near the center, where there was less distortion, while allowing more freedom in the corners. These criteria were controlled by command-line/namelist parameters so that under default values, the normal processing would take place, but the radially dependent criteria could be invoked easily in offline analysis.

2.) WISE sources to be used as candidate matches to 2MASS sources were selected after sorting on color instead of magnitude. The use of color allowed a bias toward stellar WISE detections; another desired bias toward brighter sources resulted automatically from the fact that sources have to be multi-band in order to have colors. Color was defined as the magnitude difference between the shortest and longest wavelengths detected.

Off-line programs written to modify RvB files before use by gnDSTR:

1.) In order to get meaningful results for the linear coefficients generated by gnDSTR, it is necessary to have a very large number of RvB entries for each band generated using the same *a priori* scale factors. The RvB files generated by SFPRex in QA mode (normally a 20-parameter fit) are not useful, since the scales are fitted separately for each frame. This could be overcome by just doing a 12-parameter fit in QA mode, keeping the scales frozen at their *a priori* values. As it turns out, there is a better way which has the added advantage of allowing use of the resulting RvB files to compute the band-to-band translation and rotation differences. A new off-line program RERrvb was written which, using the QA RvB files and the 3-parameter band-frame solutions, generates a set of RvB files ("RvB_3p") as they would have looked had they been generated by SFPRex in 3-parameter mode.

2.) A second off-line program TRSrvb was written to modify the RvB_3p files further. It is capable of up to a 5-parameter linearization and other manipulations to facilitate the iterative process mentioned earlier.

Changes made to the gnDSTR code were as follows.

1.) A limit on absolute residual relative to the first-pass fit was installed (gnDSTR uses two fitting passes; samples with residual chi-squares above a threshold are omitted from the second-pass fit; another filter on absolute deviation in pixel units was added).

2.) Radially dependent extra weighting was installed as an option; this allowed the fitting weight of an RvB pair to be increased as a function of distance from the center.

The first gnDSTR item was needed because RvB offsets caused by distortion were not taken into account in the position uncertainties of the WISE extractions. With fully calibrated distortion, this error should be negligible relative to the ordinary centroid estimation error, so a distortion contribution to position uncertainty was not planned. But with significant uncalibrated distortion, the RvB offsets could be large relative to the uncertainty, and this had to be prevented from causing a legitimate RvB pair from being rejected from the fit. But loosening the chi-square threshold alone tended to allow unreasonably large offsets in pixel units, as may be seen in the residuals image above, hence an absolute pixel-difference threshold was also needed.

The second gnDSTR item compensated for the sparser coverage in the array corners. With each iteration, the distortion model allowed better completeness and reliability in collecting RvB pairs, and eventually the array coverage became uniform, after which these special gnDSTR options were not needed except in W4, where the total density of RvB pairs is naturally much smaller than in the other bands. Typical values for these special options were absolute pixel deviation limits of 1 pixel in W4, 2 pixels in all other bands (hence the same angular value of about 5.5 arcsec) and weighting increasing radially to a factor of 10 in the corners (i.e., inverse variance scaled by 10).

4. Final Results

The distortion vector-flow diagrams for the current model coefficients are shown below (the zeroth order is suppressed) . These models are based on the following sample sizes of RvB pairs:

W1: 10350744
W2: 11213542
W3: 3765817
W4: 315505

The four bands are generally very similar but do have significant differences. The vector scale factor is 10. Vectors flow from array pixel location to corresponding sky location mapped onto the array through the optics.

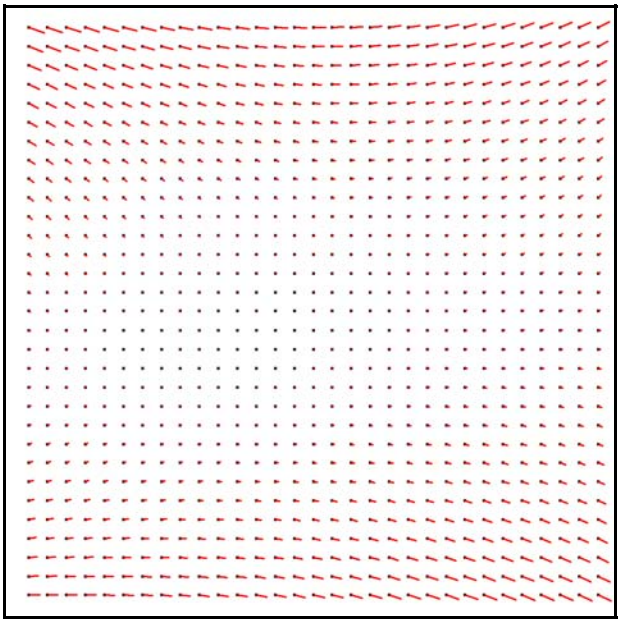

W1, Max = 2.931 pix

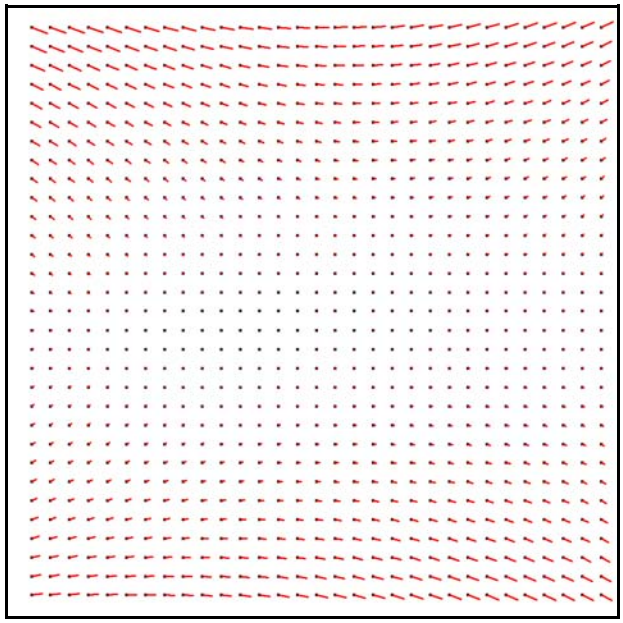

W2, Max = 3.048 pix

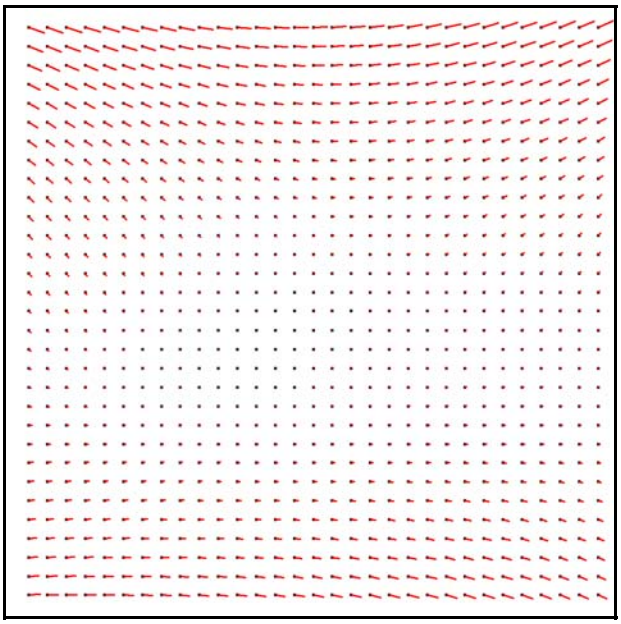

W3, Max = 3.004 pix

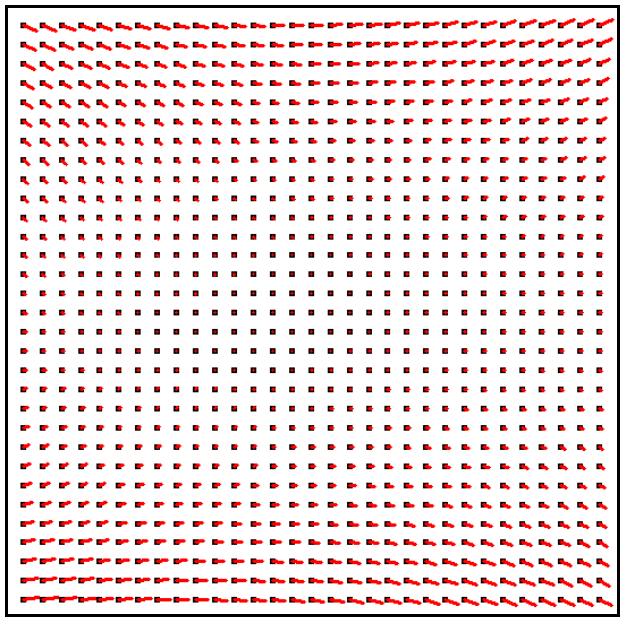

W4, Max = 1.435 pix

The W4 vectors are double-thick because the image has been scaled up to match the other bands; this restores the relative lengths to the same scale in arcseconds for all bands. The distortion is similar to the Code V model provided the latter is rotated by 270 degrees. This is shown below.

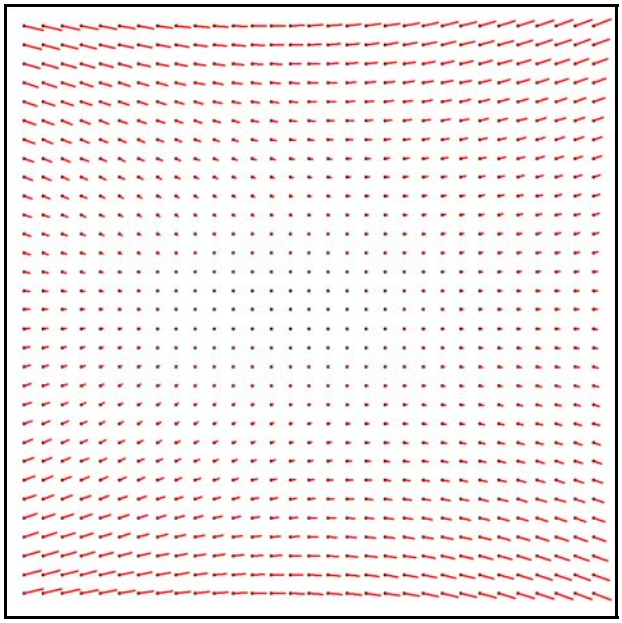

Code V Rotated 270 degrees, Max = 3.513 pix

The Code V model (rotated and with zeroth-order terms suppressed) appears to the eye to be almost the same as the calibration results, which in turn appear to be almost the same as each other. These apparent similarities are not close enough, however, to satisfy the mission requirements on position reconstruction. To illustrate this, the difference vectors for W2-W1, W3-W1, and W4-W1 are shown below with an expanded scale of 50×. W4-W1 is shown in W1 pixel units.

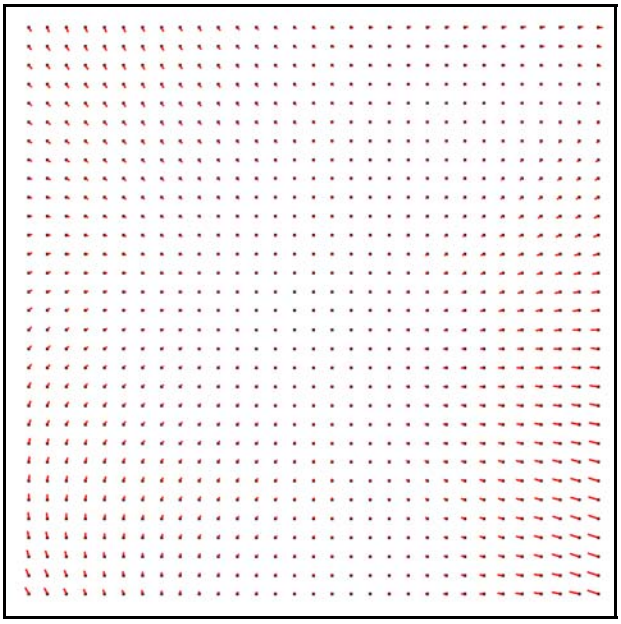

W2-W1, Max = 0.398 pix

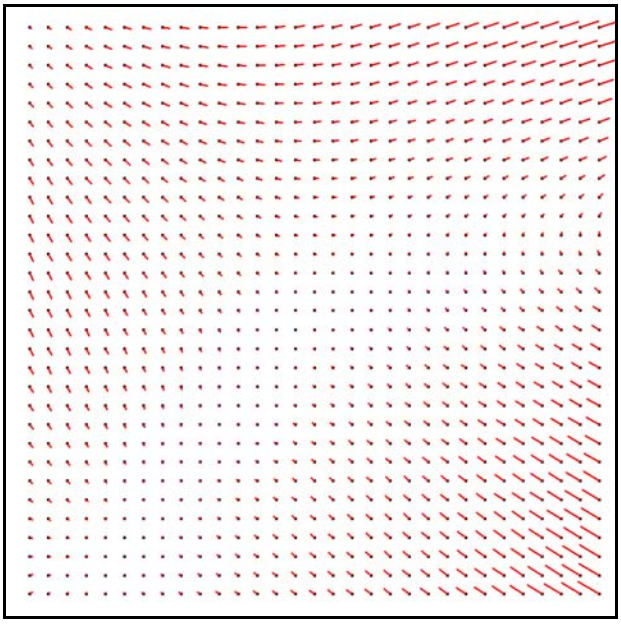

W3-W1, Max = 0.876 pix

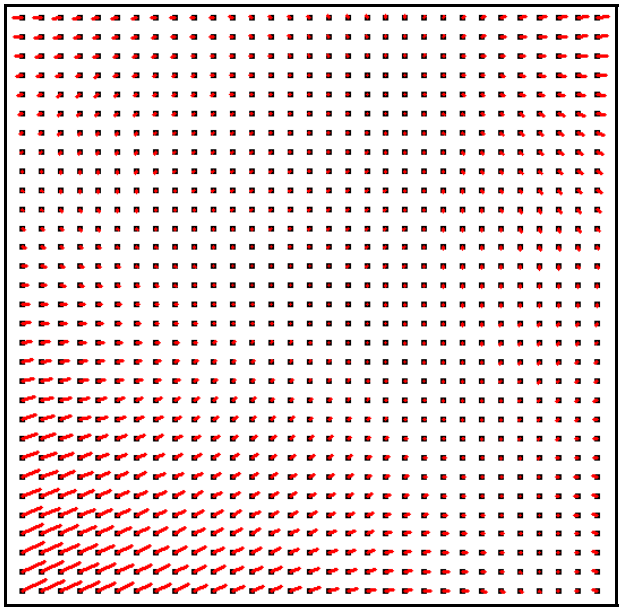

W4-W1, Max = 0.940 pix

The bands are more similar to each other than to the Code V model, as seen in the difference-vector diagrams below, which are shown with the smaller scale fact of 20×. W4 employs W4 pixel units.

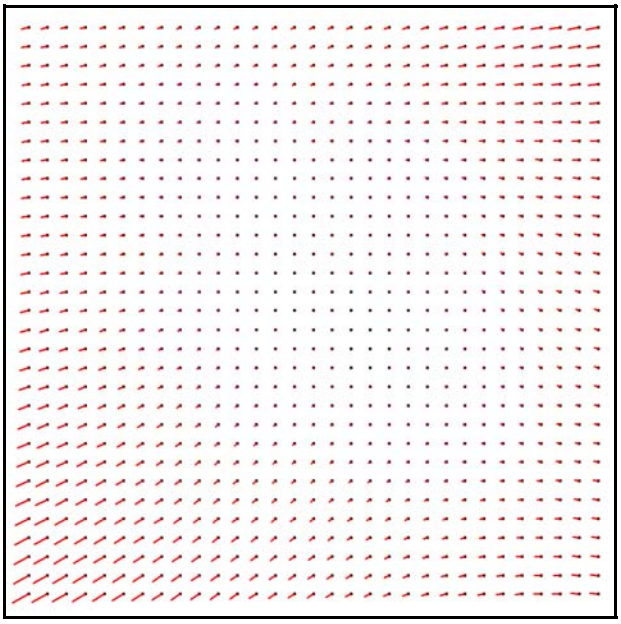

W1-CodeV, Max = 1.640 pix

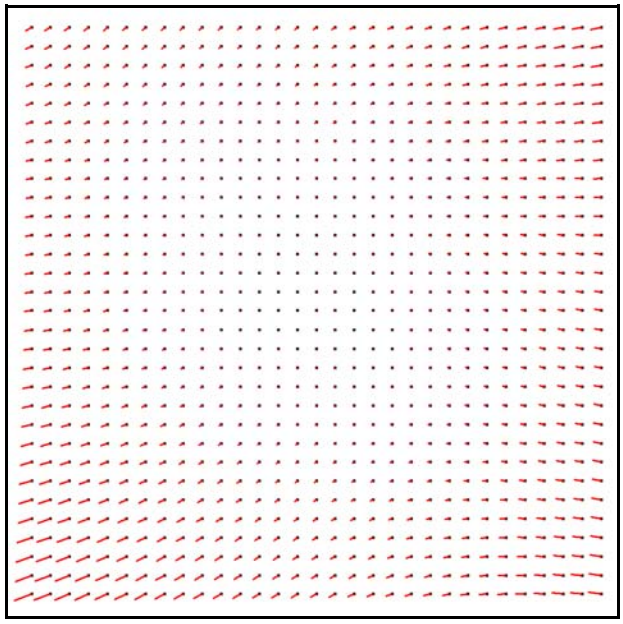

W2-CodeV, Max = 1.658 pix

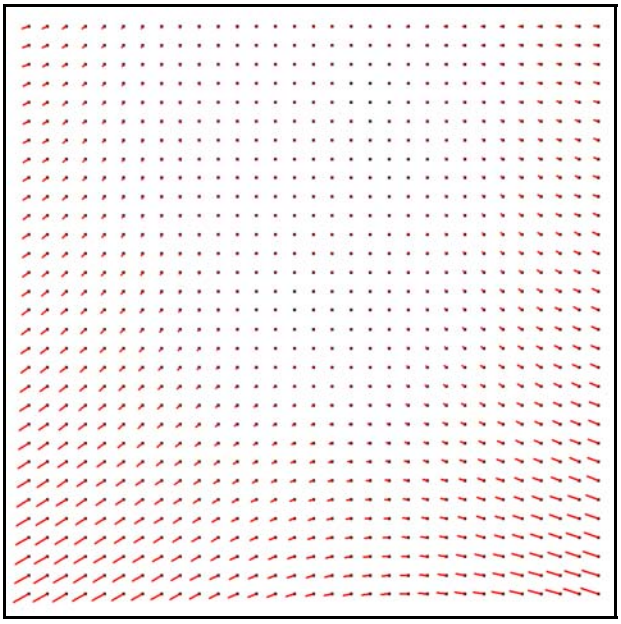

W3-CodeV, Max = 1.605 pix

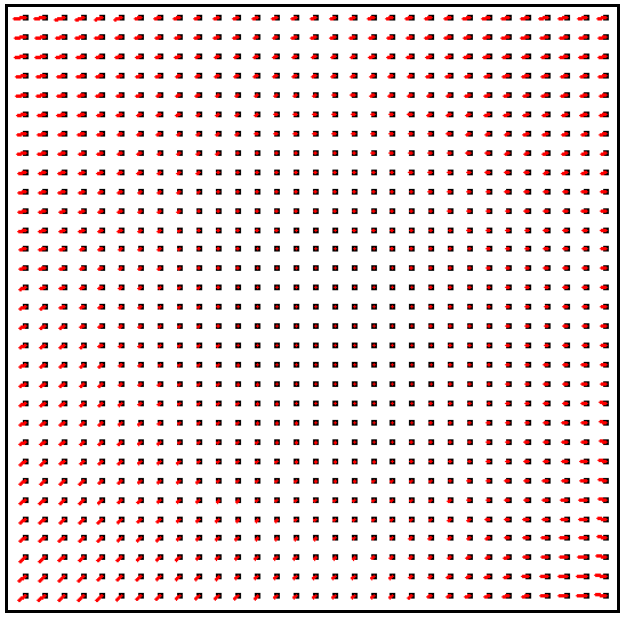

W4-CodeV, Max = 0.976 pix

Plots presenting RvB X and Y position discrepancy histograms provide further insight into this issue. For each band, residuals are computed and histogrammed for three cases: (a.) no distortion correction (shown in blue); (b.) distortion corrected with the rotated Code V model (shown in green); (c.) the final flight-data-derived distortion model (red). Note that while the Code V model provides a definite improvement over no distortion correction, it falls well short of what was achieved via fitting the flight data. The improvement is most noticeable for the shorter-wavelength bands where many more RvB pairs are available, also having tighter WISE position uncertainties. In keeping with this, W4 shows the least improvement.

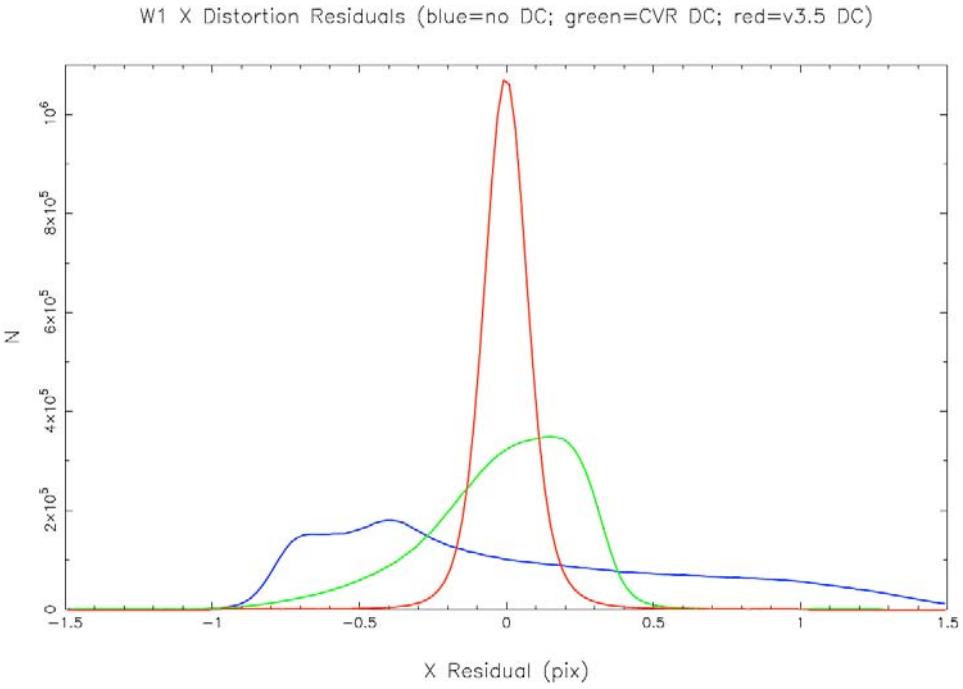

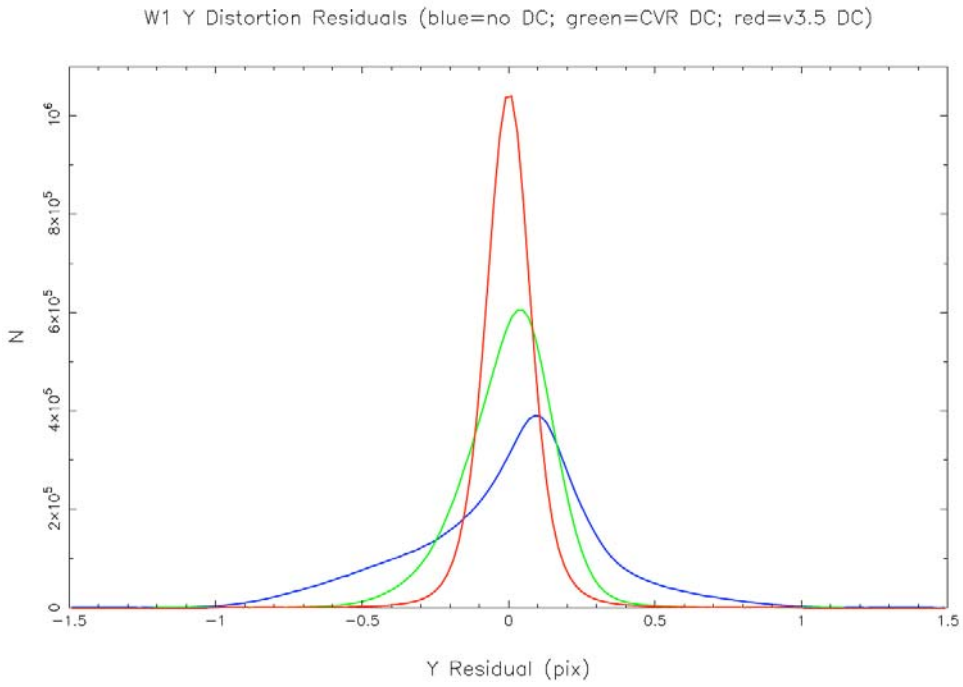

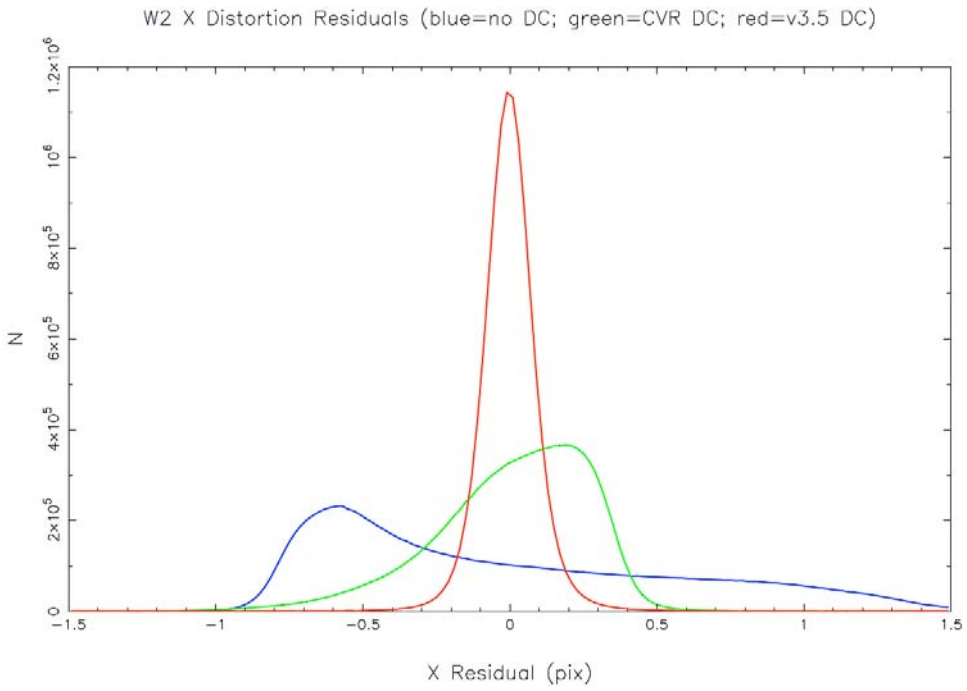
W2 X Distortion Residuals (blue=no DC; green=CVR DC; red=v3.5 DC)
N
X Residual (pix)
0
2×10^5
4×10^5
6×10^5
8×10^5
10^6
1.2×10^6
−1.5
−1
−0.5
0
0.5
1
1.5

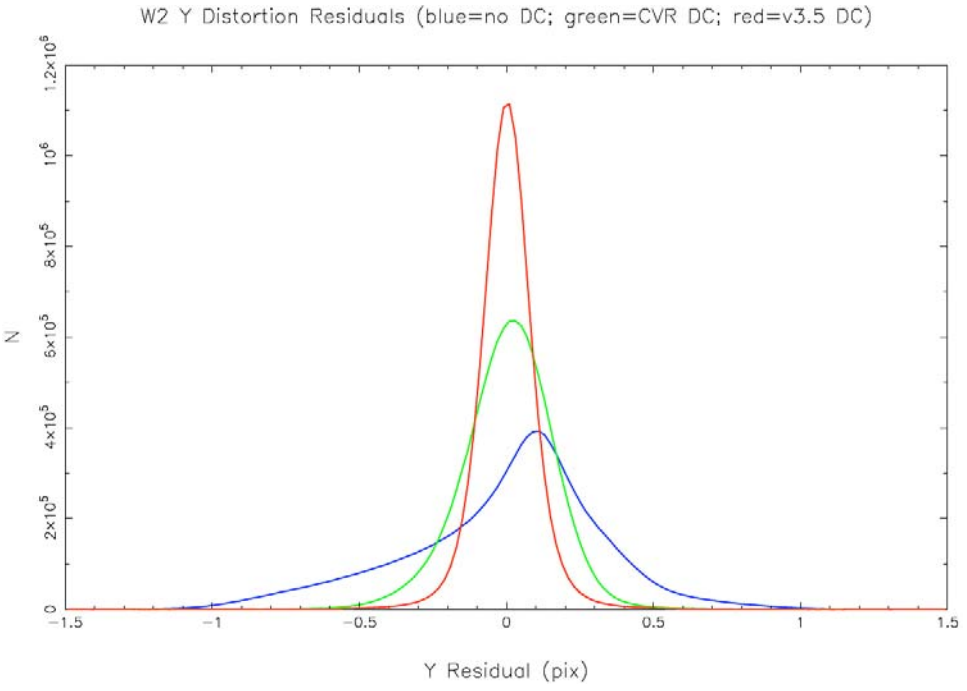
W2 Y Distortion Residuals (blue=no DC; green=CVR DC; red=v3.5 DC)
N
Y Residual (pix)
0
2×10^5
4×10^5
6×10^5
8×10^5
10^6
1.2×10^6
−1.5
−1
−0.5
0
0.5
1
1.5

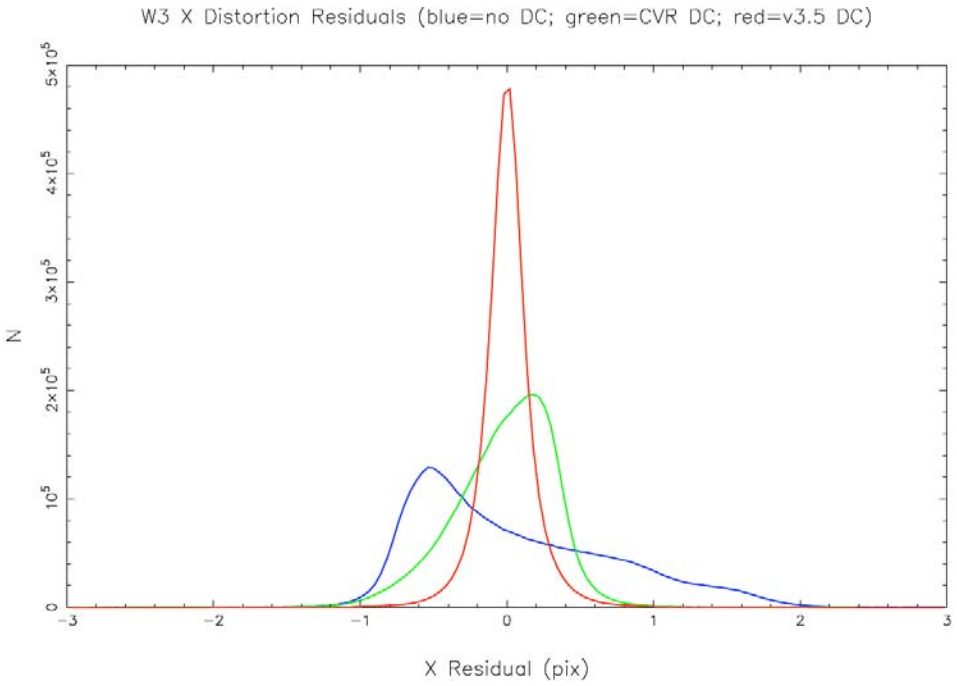
W3 X Distortion Residuals (blue=no DC; green=CVR DC; red=v3.5 DC)
N
X Residual (pix)

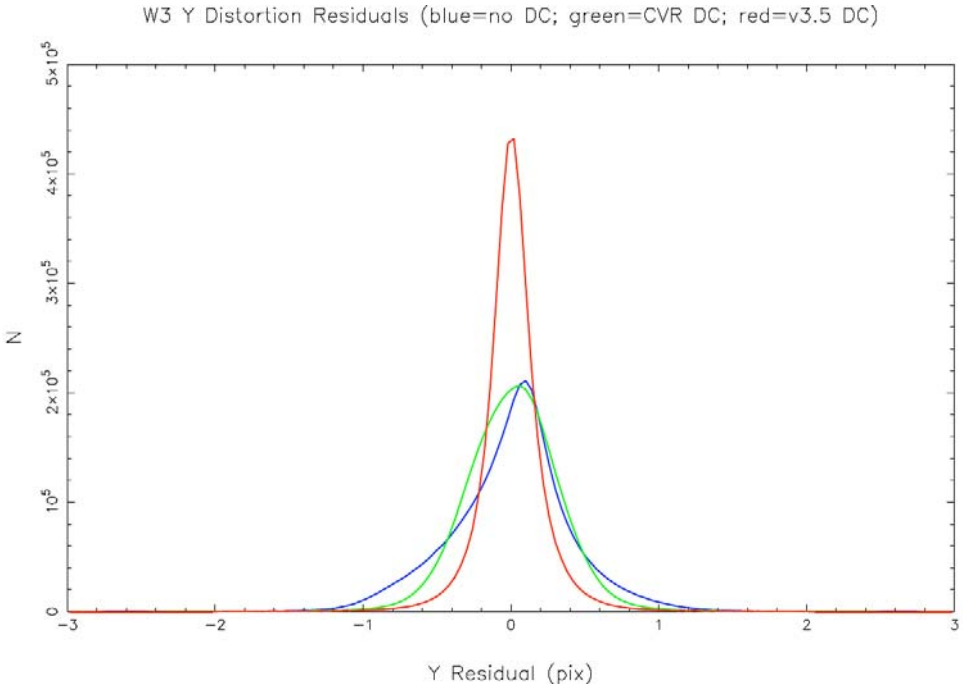
W3 Y Distortion Residuals (blue=no DC; green=CVR DC; red=v3.5 DC)
N
Y Residual (pix)

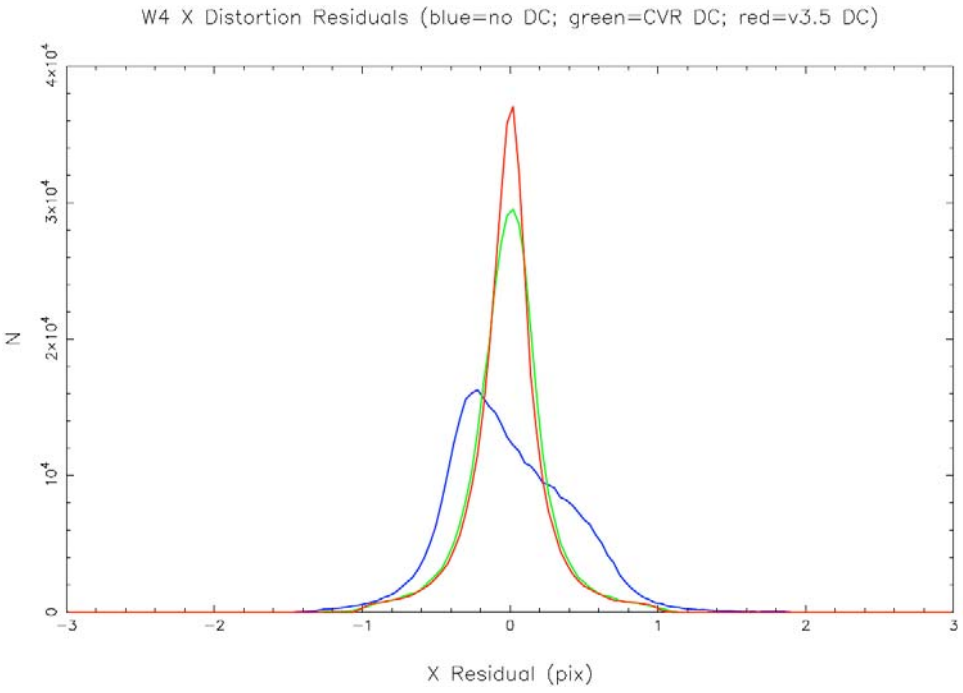
W4 X Distortion Residuals (blue=no DC; green=CVR DC; red=v3.5 DC)
N
X Residual (pix)

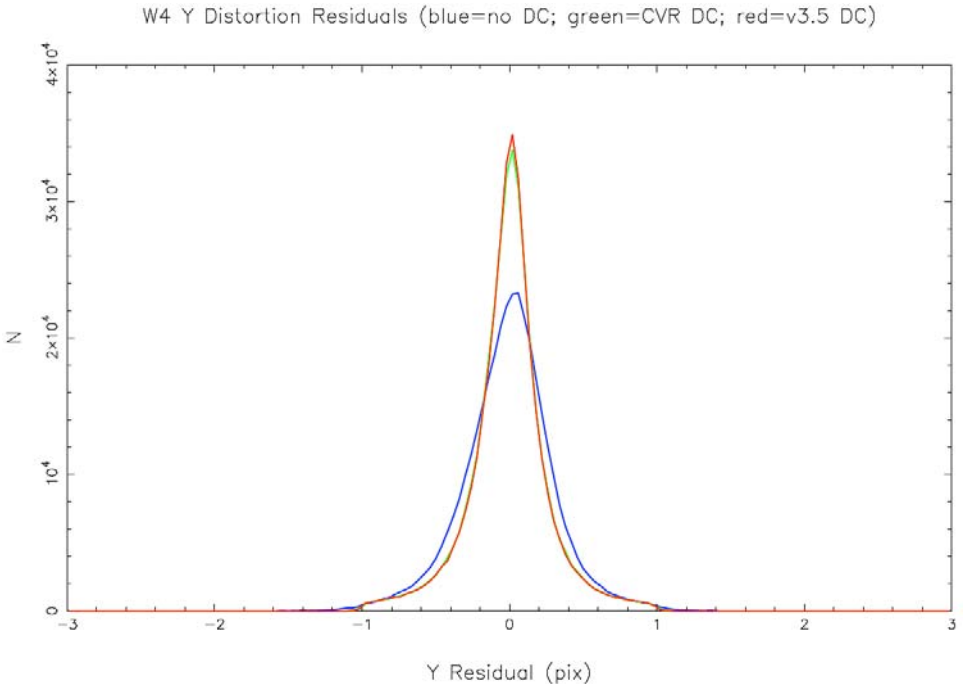
W4 Y Distortion Residuals (blue=no DC; green=CVR DC; red=v3.5 DC)
N
Y Residual (pix)

5. Analysis of Residuals

Since the WISE extraction position errors contribute to the dispersion in the fitting residuals, a set of 31×31 array-binned average residuals and the dispersions over the bins were computed (i.e., the arrays were partitioned into 31 approximately equal segments per axis, and average WISE-2MASS position discrepancies were computed separately in the these bins based on source location; then dispersions over the bins were computed). These mean and sigma residuals should be more typical of the distortion model's actual fitting error, and are as follows, where the units are pixels.

Band/Axis	Mean	Sigma	Min	Max	Median	1%-tile	99%-tile
W1/X	0.002070	0.01949	-0.08298	0.06435	0.002512	-0.04942	0.04579
W1/Y	-0.009074	0.01159	-0.04935	0.04348	-0.00373	-0.03837	0.0251
W1/radial	0.10500	0.01133	0.08822	0.1532	0.1024	0.08905	0.1389
W2/X	0.002548	0.01679	-0.05003	0.03995	0.003702	-0.03939	0.03376
W2/Y	0.01571	0.008914	-0.00831	0.09537	0.01525	-0.003964	0.04101
W2/radial	0.1153	0.008315	0.1003	0.1602	0.1141	0.1023	0.1402
W3/X	0.001249	0.01608	-0.07536	0.06285	0.000749	-0.04667	0.03709
W3/Y	0.003491	0.008846	-0.02428	0.05594	0.003343	-0.01592	0.02558
W3/radial	0.2993	0.01451	0.2736	0.3576	0.2971	0.2765	0.3421
W4/X	-0.003836	0.0236	-0.07924	0.07422	-0.004239	-0.05865	0.04831
W4/Y	0.000638	0.02276	-0.07615	0.08211	0.001318	-0.05045	0.05234
W4/radial	0.4832	0.0156	0.4345	0.5377	0.4829	0.4487	0.5187

Table 5-1. Distortion Fitting Residuals (31×31 bins, pixel units)

The distributions of these residuals over the arrays revealed that the distortion fit was good enough so that the limiting effects include a significant contribution produced by the 5×5 partitioning of the array into PSF segments for use in modeling point-source template variation over the array. The very small interpolation residuals produced a clear 5×5 partitioning of the residual images in W1 and W2, as shown on the next page. The effect is not evident in W3, where the partitioning appears as a 2×2 effect, and no subdivision is obvious in W4. There appears to be some contribution from the polynomial residuals as well, since the X residuals show two vertical stripes in W1, W2, and W3, where the latter has the same stripes despite the absence of the 5×5 partitioning. In any case, these residuals are very small and well under the requirements for point-source position reconstruction.

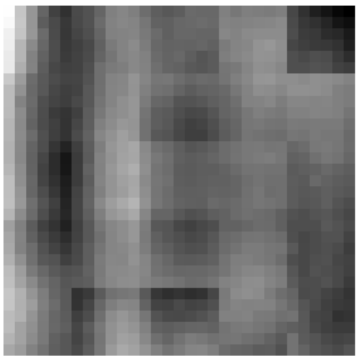

W1 X Residuals

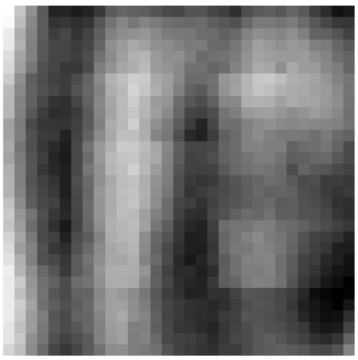

W2 X Residuals

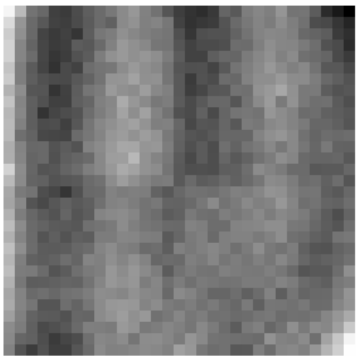

W3 X Residuals

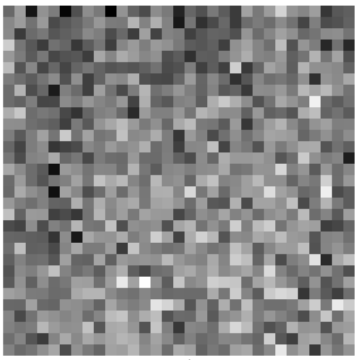

W4 X Residuals

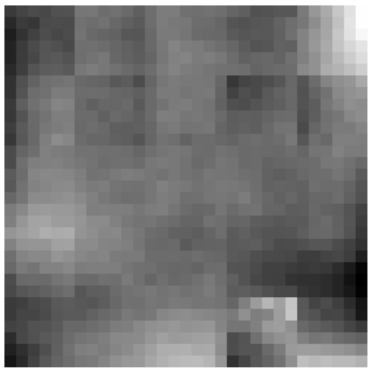

W1 Y Residuals

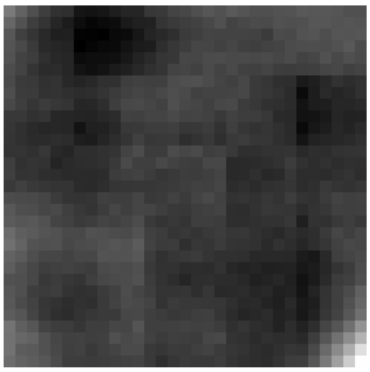

W2 Y Residuals

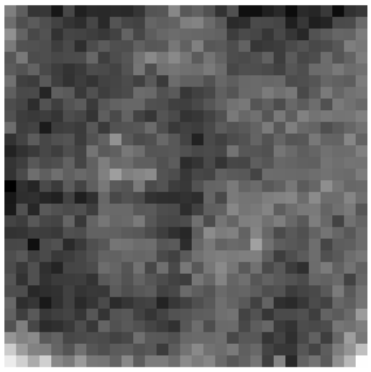

W3 Y Residuals

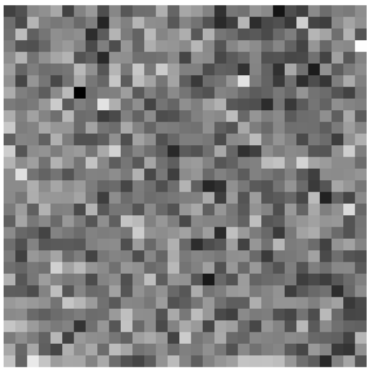

W4 Y Residuals

The point-source band-to-band alignment error will contain a contribution from the distortion residuals. For a single frameset, the bands are always registered the same way relative to each other, and so the distortion model's contribution to this alignment error will be the difference in distortion residual. This difference is generally smaller than the single-band residuals because of the correlated band-to-band error. The residual statistics for single-frameset band-to-band alignment are shown below, where the units are arcsec so that band pairs with W4 can be included..

Bands/Axis	Mean	Sigma	Min	Max	Median	1%-tile	99%-tile
W2-W1/X	0.00052	0.03326	-0.1078	0.09478	0.000037	-0.09063	0.08506
W2-W1/Y	0.05974	0.03211	-0.04772	0.1874	0.05815	-0.01593	0.1630
W3-W1/X	-0.003054	0.04556	-0.2649	0.1186	-0.000803	-0.1474	0.08938
W3-W1/Y	0.02614	0.03602	-0.1187	0.2176	0.02591	-0.05655	0.1174
W4-W1/X	-0.03016	0.1339	-0.4757	0.4248	-0.03325	-0.3536	0.2691
W4-W1/Y	0.01859	0.1267	-0.3999	0.4230	0.1710	-0.2721	0.3172
W3-W2/X	-0.003574	0.04361	-0.2090	0.1282	0.000165	-0.1413	0.08150
W3-W2/Y	-0.03360	0.03034	-0.1408	0.04692	-0.03316	-0.1147	0.02745
W4-W2/X	-0.03068	0.1339	-0.4978	0.3718	-0.03169	-0.3679	0.2731
W4-W2/Y	-0.04080	0.1273	-0.4553	0.3888	-0.03699	-0.3401	0.2463
W4-W3/X	-0.02711	0.1257	-0.4398	0.3993	-0.02883	-0.3322	0.2591
W4-W3/Y	-0.007193	0.1258	-0.4086	0.4141	-0.005563	-0.2878	0.2811

Table 5-2. Single-Frameset Band-to-Band Alignment Residuals (arcsec)

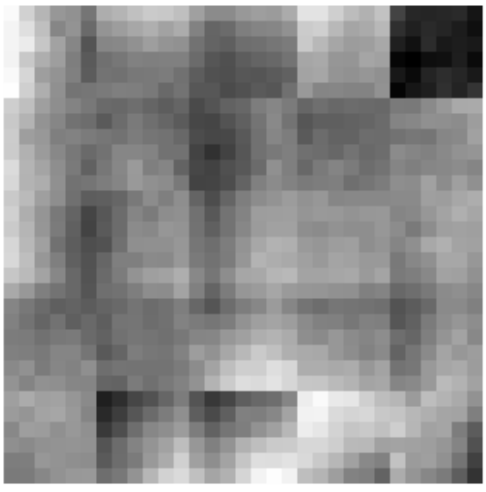

W2-W1 X Residuals

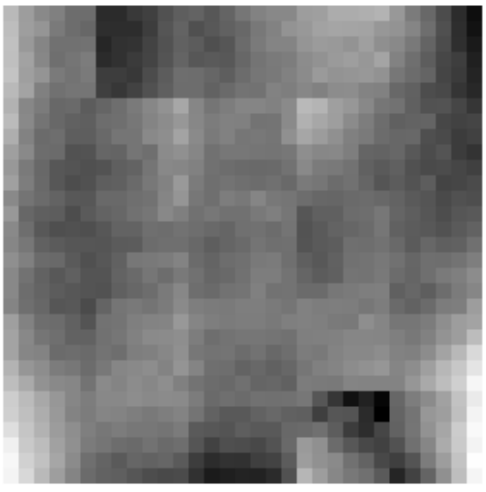

W2-W1 Y Residuals

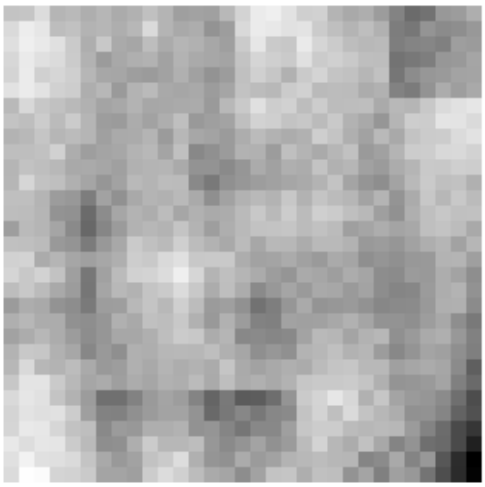

W3-W1 X Residuals

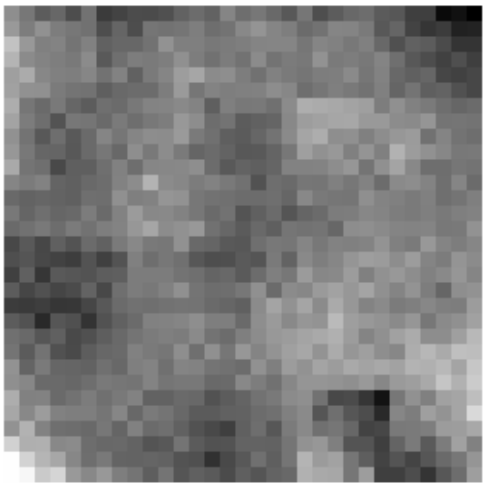

W3-W1 Y Residuals

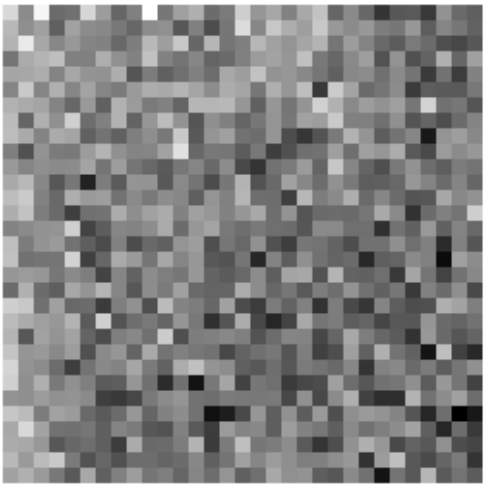

W4-W1 X Residuals

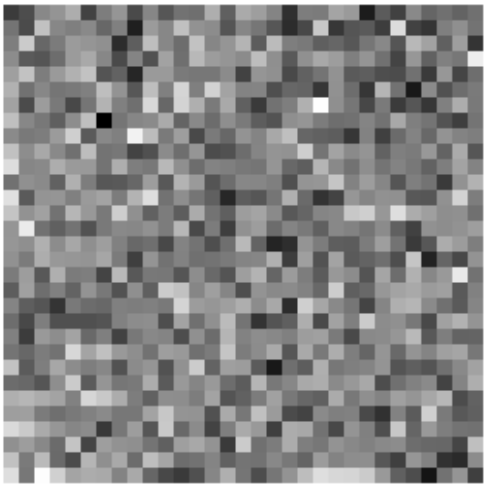

W4-W1 Y Residuals

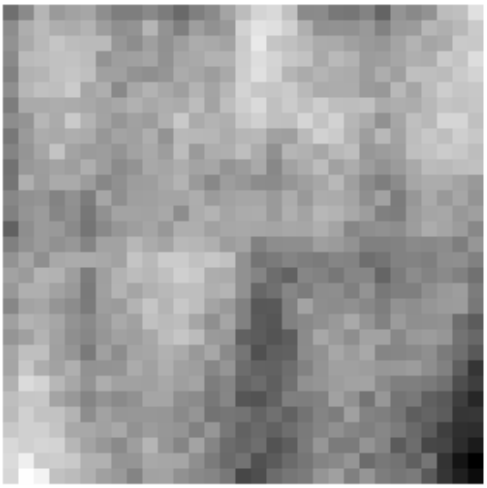

W3-W2 X Residuals

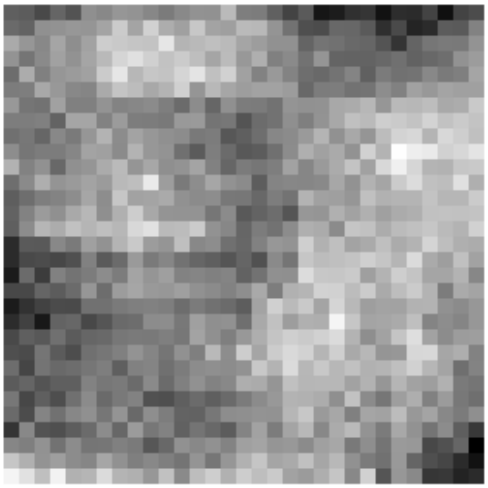

W3-W2 Y Residuals

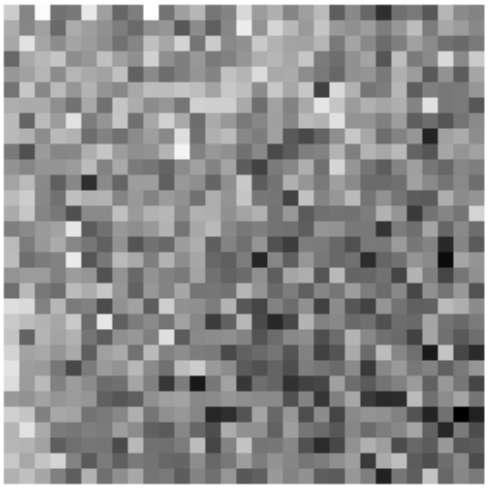

W4-W2 X Residuals

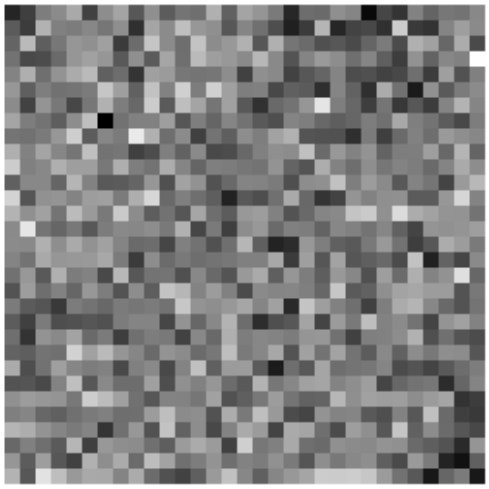

W4-W2 Y Residuals

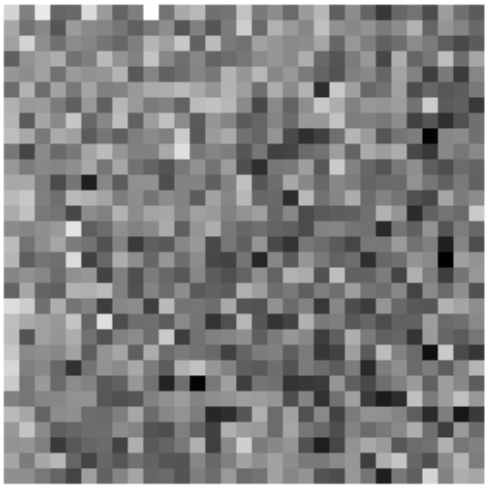

W4-W3 X Residuals

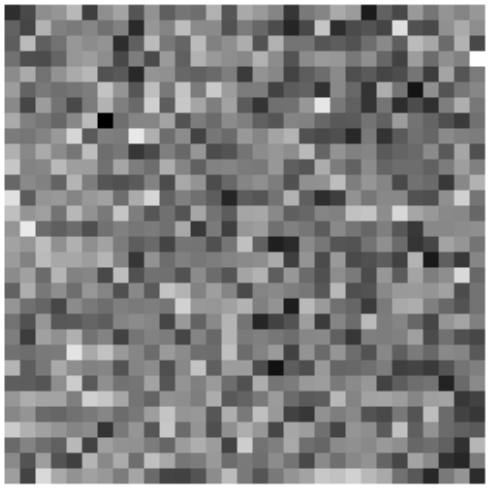

W4-W3 Y Residuals

For multi-frame images, the single-band residuals will be free to align in any possible overlap, including each band with itself. To estimate the amount of blurring to be expected from distortion-correction residuals, the following in-band smearing analysis was performed (band-to-band smearing should be generally similar and was not analyzed, but the in-band analysis could be extended to include band-to-band if requested).

The residuals are converted from pixel units to arcseconds, after which each band/axis combination is treated identically, and so we will limit the discussion to a single band and a single axis. All 961×961 combinations of residual alignments are used to computed the residual difference. This produces a 961×961 antisymmetric array of residual differences. The statistics of each band's X and Y alignment residuals are obtained from these arrays. The means and medians are all zero because the arrays are anti-symmetric, i.e., the set of all possible pixel-pair differences includes each pixel once as the minuend and once as the subtrahend in each pair. For this reason, the minima and

maxima are of equal magnitude and opposite sign, as are the 1st and 99th percentiles.

Band/Axis	Mean	Sigma	Min	Max	Median	1%-tile	99%-tile
W1/X	0.0	0.2073	-1.111	1.111	0.0	-0.5059	0.5059
W1/Y	0.0	0.0388	-0.1982	0.1982	0.0	-0.1005	0.1005
W2/X	0.0	0.06531	-0.2474	0.2474	0.0	-0.1471	0.1471
W2/Y	0.0	0.03467	-0.2851	0.2851	0.0	-0.08801	0.08801
W3/X	0.0	0.06256	-0.3801	0.3801	0.0	-0.1546	0.1546
W3/Y	0.0	0.03440	-0.2206	0.2206	0.0	-0.0829	0.0829
W4/X	0.0	0.1811	-0.8310	0.8310	0.0	-0.4249	0.4249
W4/Y	0.0	0.1764	-0.8766	0.8766	0.0	-0.4102	0.4102

Table 5-3. In-Band Multiframe Alignment Residuals (arcsec)

All of the values of residuals shown above are in fact slightly overestimated because of the fact that the gnDSTR program outputs residuals relative to the first-pass fit, and excluding samples with residuals above threshold causes the second-pass fit to yield a better model (which is why the two-pass fitting is done). However, as the iterative solution for the best models progressed, each new first-pass fit was closer to that of the second pass, as evidenced by the reduced number of outliers rejected. So these final estimates of residuals should be only slightly overestimated, and in fact the amount of overestimation may be dominated by the extraction position error, which is averaged down but not driven to zero.

6. Formal Uncertainties

The formal uncertainties of the distortion models were computed and represented as vector-flow diagrams, where the vectors extend from the nominal array location to the four points defined by all combinations of the offsets $\pm 1\sigma_x$ and $\pm 1\sigma_y$ with a scale factor of 2000.

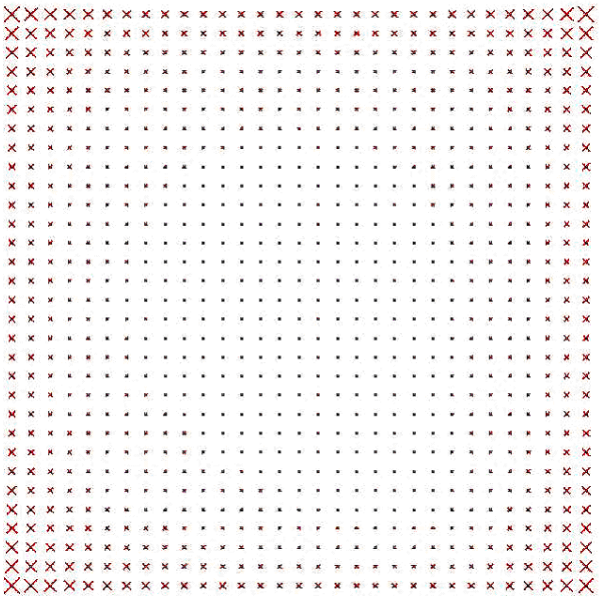

W1 Uncertainties (max radius 0.0093 pix)

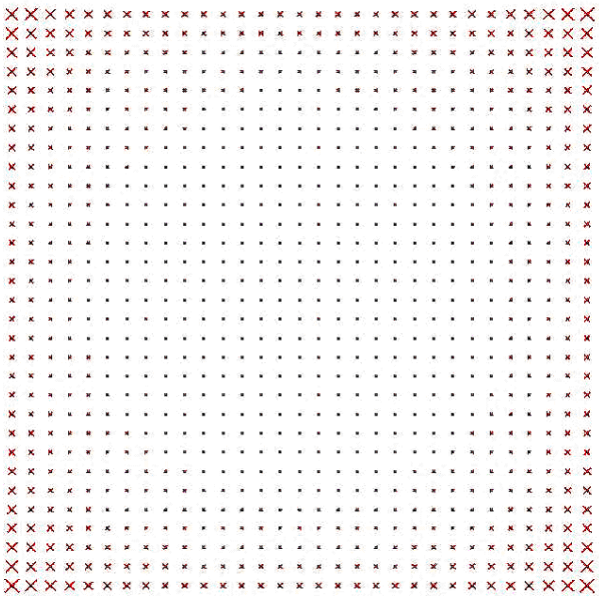

W2 Uncertainties (max radius 0.0082 pix)

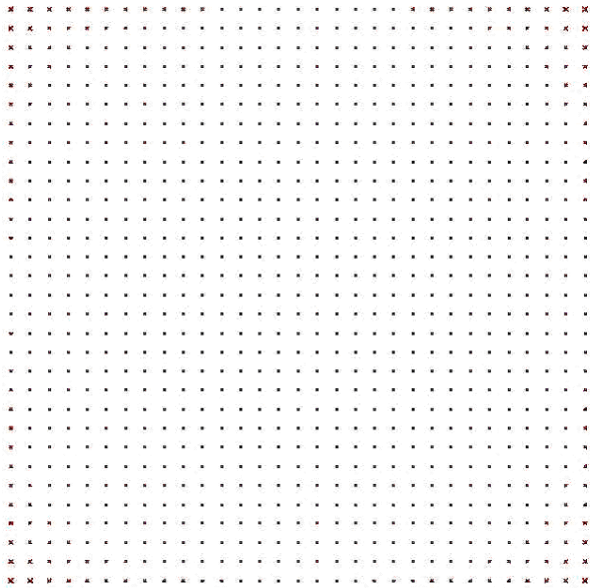

W3 Uncertainties (max radius 0.0028 pix)

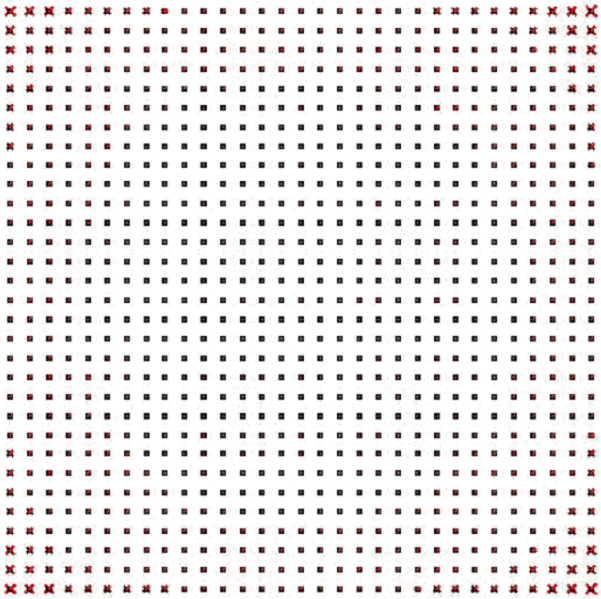

W4 Uncertainties (max radius 0.0026 pix)

Appendix A: Effects of Frame Rotation On SIP Coefficients

The Code V distortion pattern was analyzed with rotations through 90, 180, and 270 degrees. The SIP coefficients for all four orientations were then related to each other. A summary of these relationships is given below.

R=0	R=90	R=180	R=270
A_0_2	-B_2_0	-A_0_2	B_2_0
A_0_3	-B_3_0	A_0_3	-B_3_0
A_0_4	-B_4_0	-A_0_4	B_4_0
A_1_1	B_1_1	-A_1_1	-B_1_1
A_1_2	B_2_1	A_1_2	B_2_1
A_1_3	B_3_1	-A_1_3	-B_3_1
A_2_0	-B_0_2	-A_2_0	B_0_2
A_2_1	-B_1_2	A_2_1	-B_1_2
A_2_2	-B_2_2	-A_2_2	B_2_2
A_3_0	B_0_3	A_3_0	B_0_3
A_3_1	B_1_3	-A_3_1	-B_1_3
A_4_0	-B_0_4	-A_4_0	B_0_4
A_DMAX	B_DMAX	A_DMAX	B_DMAX
B_0_2	A_2_0	-B_0_2	-A_2_0
B_0_3	A_3_0	B_0_3	A_3_0
B_0_4	A_4_0	-B_0_4	-A_4_0
B_1_1	-A_1_1	-B_1_1	A_1_1
B_1_2	-A_2_1	B_1_2	-A_2_1
B_1_3	-A_3_1	-B_1_3	A_3_1
B_2_0	A_0_2	-B_2_0	-A_0_2
B_2_1	A_1_2	B_2_1	A_1_2
B_2_2	A_2_2	-B_2_2	-A_2_2
B_3_0	-A_0_3	B_3_0	-A_0_3
B_3_1	-A_1_3	-B_3_1	A_1_3
B_4_0	A_0_4	-B_4_0	-A_0_4
B_DMAX	A_DMAX	B_DMAX	A_DMAX
AP_0_2	-BP_2_0	-AP_0_2	BP_2_0
AP_0_3	-BP_3_0	AP_0_3	-BP_3_0
AP_0_4	-BP_4_0	-AP_0_4	BP_4_0
AP_1_1	BP_1_1	-AP_1_1	-BP_1_1
AP_1_2	BP_2_1	AP_1_2	BP_2_1
AP_1_3	BP_3_1	-AP_1_3	-BP_3_1
AP_2_0	-BP_0_2	-AP_2_0	BP_0_2
AP_2_1	-BP_1_2	AP_2_1	-BP_1_2
AP_2_2	-BP_2_2	-AP_2_2	BP_2_2
AP_3_0	BP_0_3	AP_3_0	BP_0_3
AP_3_1	BP_1_3	-AP_3_1	-BP_1_3
AP_4_0	-BP_0_4	-AP_4_0	BP_0_4
BP_0_2	AP_2_0	-BP_0_2	-AP_2_0
BP_0_3	AP_3_0	BP_0_3	AP_3_0
BP_0_4	AP_4_0	-BP_0_4	-AP_4_0
BP_1_1	-AP_1_1	-BP_1_1	AP_1_1
BP_1_2	-AP_2_1	BP_1_2	-AP_2_1
BP_1_3	-AP_3_1	-BP_1_3	AP_3_1
BP_2_0	AP_0_2	-BP_2_0	-AP_0_2
BP_2_1	AP_1_2	BP_2_1	AP_1_2
BP_2_2	AP_2_2	-BP_2_2	-AP_2_2
BP_3_0	-AP_0_3	BP_3_0	-AP_0_3
BP_3_1	-AP_1_3	-BP_3_1	AP_1_3
BP_4_0	AP_0_4	-BP_4_0	-AP_0_4

The AP and BP values are functions of each other that follow the same pattern as the A and B values. The latter can be expressed as follows.

R=0	R=90	R=180	R=270
A_I_J	S_{A90}×B_J_I	S_{A180}×A_I_J	S_{A270}×B_J_I
	S_{A90} = -1 for I even else +1 (I = 2nd index)	S_{A180} = -1 for I+J even else +1	S_{A270} = -1 for J odd else +1 (J = 1st index)
B_I_J	S_{B90}×A_J_I	S_{B180}×B_I_J	S_{B270}×A_J_I
	S_{B90} = -1 for I odd else +1 (I = 2nd index)	S_{B180} = -1 for I+J even else +1	S_{B270} = -1 for J even else +1 (J = 1st index)

Appendix B: Current SIP Coefficients Meta-Data For Ops

The current values of the SIP coefficients as used by the ops pipeline processing are in a meta-data file containing the following distortion-related entries.

```
\
\ w1
\cal:gnd:distort_skew       1     SKEW       r        0.000000E+00  [rad] skew component of CD matrix
 cal:gnd:distort_a_order    1     A_ORDER    i                   4  polynomial order, axis 1, detector to sky
 cal:gnd:distort_a_0_0      1     A_0_0      r        7.228039E-01  axis 1 distortion coefficient of v0
 cal:gnd:distort_a_0_1      1     A_0_1      r       -1.243220E-04  axis 1 distortion coefficient of v1
 cal:gnd:distort_a_1_0      1     A_1_0      r       -7.790246E-04  axis 1 distortion coefficient of u1
 cal:gnd:distort_a_0_2      1     A_0_2      r       -7.793528E-06  axis 1 distortion coefficient of v2
 cal:gnd:distort_a_0_3      1     A_0_3      r       -2.928111E-10  axis 1 distortion coefficient of v3
 cal:gnd:distort_a_0_4      1     A_0_4      r       -6.270019E-13  axis 1 distortion coefficient of v4
 cal:gnd:distort_a_1_1      1     A_1_1      r        1.344445E-06  axis 1 distortion coefficient of u.v
 cal:gnd:distort_a_1_2      1     A_1_2      r        1.228555E-09  axis 1 distortion coefficient of u.v2
 cal:gnd:distort_a_1_3      1     A_1_3      r       -5.895443E-13  axis 1 distortion coefficient of u.v3
 cal:gnd:distort_a_2_0      1     A_2_0      r       -1.629945E-06  axis 1 distortion coefficient of u2
 cal:gnd:distort_a_2_1      1     A_2_1      r       -1.186318E-10  axis 1 distortion coefficient of u2.v
 cal:gnd:distort_a_2_2      1     A_2_2      r        1.503974E-12  axis 1 distortion coefficient of u2.v2
 cal:gnd:distort_a_3_0      1     A_3_0      r        2.756392E-09  axis 1 distortion coefficient of u3
 cal:gnd:distort_a_3_1      1     A_3_1      r       -4.586393E-13  axis 1 distortion coefficient of u2.v
 cal:gnd:distort_a_4_0      1     A_4_0      r        1.794526E-12  axis 1 distortion coefficient of u4
 cal:gnd:distort_a_dmax     1     A_DMAX     r              2.046  [pixel] axis 1 maximum correction
 cal:gnd:distort_b_order    1     B_ORDER    i                   4  polynomial order, axis 2, detector to sky
 cal:gnd:distort_b_0_0      1     B_0_0      r       -7.946909E-02  axis 2 distortion coefficient of v0
 cal:gnd:distort_b_0_1      1     B_0_1      r        3.218232E-04  axis 2 distortion coefficient of v1
 cal:gnd:distort_b_1_0      1     B_1_0      r       -2.481941E-04  axis 2 distortion coefficient of u1
 cal:gnd:distort_b_0_2      1     B_0_2      r        1.165828E-06  axis 2 distortion coefficient of v2
 cal:gnd:distort_b_0_3      1     B_0_3      r       -3.174803E-09  axis 2 distortion coefficient of v3
 cal:gnd:distort_b_0_4      1     B_0_4      r       -8.545365E-13  axis 2 distortion coefficient of v4
 cal:gnd:distort_b_1_1      1     B_1_1      r       -3.541684E-06  axis 2 distortion coefficient of u.v
 cal:gnd:distort_b_1_2      1     B_1_2      r       -4.987962E-10  axis 2 distortion coefficient of u.v2
 cal:gnd:distort_b_1_3      1     B_1_3      r        1.458031E-12  axis 2 distortion coefficient of u.v3
 cal:gnd:distort_b_2_0      1     B_2_0      r       -6.590985E-08  axis 2 distortion coefficient of u2
```

```
cal:gnd:distort_b_2_1      1     B_2_1      r       -2.600160E-10  axis 2 distortion coefficient of u2.v
cal:gnd:distort_b_2_2      1     B_2_2      r       -2.594371E-13  axis 2 distortion coefficient of u2.v2
cal:gnd:distort_b_3_0      1     B_3_0      r       -6.360093E-11  axis 2 distortion coefficient of u3
cal:gnd:distort_b_3_1      1     B_3_1      r        7.028808E-13  axis 2 distortion coefficient of u2.v
cal:gnd:distort_b_4_0      1     B_4_0      r        8.797685E-13  axis 2 distortion coefficient of u4
cal:gnd:distort_b_dmax     1     B_DMAX     r               1.066  [pixel] axis 2 maximum correction
cal:gnd:distort_ap_order   1     AP_ORDER   i                   4  polynomial order, axis 1, sky to detector
cal:gnd:distort_ap_0_0     1     AP_0_0     r       -7.233219E-01  axis 1 distortion coefficient of V0
cal:gnd:distort_ap_0_1     1     AP_0_1     r        1.261763E-04  axis 1 distortion coefficient of V1
cal:gnd:distort_ap_1_0     1     AP_1_0     r        7.777227E-04  axis 1 distortion coefficient of U1
cal:gnd:distort_ap_0_2     1     AP_0_2     r        7.795772E-06  axis 1 distortion coefficient of V2
cal:gnd:distort_ap_0_3     1     AP_0_3     r        2.696271E-10  axis 1 distortion coefficient of V3
cal:gnd:distort_ap_0_4     1     AP_0_4     r        6.665114E-13  axis 1 distortion coefficient of V4
cal:gnd:distort_ap_1_1     1     AP_1_1     r       -1.342059E-06  axis 1 distortion coefficient of U.V
cal:gnd:distort_ap_1_2     1     AP_1_2     r       -1.159637E-09  axis 1 distortion coefficient of U.V2
cal:gnd:distort_ap_1_3     1     AP_1_3     r        6.084245E-13  axis 1 distortion coefficient of U.V3
cal:gnd:distort_ap_2_0     1     AP_2_0     r        1.636841E-06  axis 1 distortion coefficient of U2
cal:gnd:distort_ap_2_1     1     AP_2_1     r        1.107923E-10  axis 1 distortion coefficient of U2.V
cal:gnd:distort_ap_2_2     1     AP_2_2     r       -1.580363E-12  axis 1 distortion coefficient of U2.V2
cal:gnd:distort_ap_3_0     1     AP_3_0     r       -2.759976E-09  axis 1 distortion coefficient of U3
cal:gnd:distort_ap_3_1     1     AP_3_1     r        4.712913E-13  axis 1 distortion coefficient of U2.V
cal:gnd:distort_ap_4_0     1     AP_4_0     r       -1.804259E-12  axis 1 distortion coefficient of U4
cal:gnd:distort_bp_order   1     BP_ORDER   i                   4  polynomial order, axis 2, sky to detector
cal:gnd:distort_bp_0_0     1     BP_0_0     r        7.930997E-02  axis 2 distortion coefficient of V0
cal:gnd:distort_bp_0_1     1     BP_0_1     r       -3.239962E-04  axis 2 distortion coefficient of V1
cal:gnd:distort_bp_1_0     1     BP_1_0     r        2.484437E-04  axis 2 distortion coefficient of U1
cal:gnd:distort_bp_0_2     1     BP_0_2     r       -1.163635E-06  axis 2 distortion coefficient of V2
cal:gnd:distort_bp_0_3     1     BP_0_3     r        3.198763E-09  axis 2 distortion coefficient of V3
cal:gnd:distort_bp_0_4     1     BP_0_4     r        8.509823E-13  axis 2 distortion coefficient of V4
cal:gnd:distort_bp_1_1     1     BP_1_1     r        3.542573E-06  axis 2 distortion coefficient of U.V
cal:gnd:distort_bp_1_2     1     BP_1_2     r        4.895069E-10  axis 2 distortion coefficient of U.V2
cal:gnd:distort_bp_1_3     1     BP_1_3     r       -1.423222E-12  axis 2 distortion coefficient of U.V3
cal:gnd:distort_bp_2_0     1     BP_2_0     r        6.524476E-08  axis 2 distortion coefficient of U2
cal:gnd:distort_bp_2_1     1     BP_2_1     r        2.734704E-10  axis 2 distortion coefficient of U2.V
cal:gnd:distort_bp_2_2     1     BP_2_2     r        2.664114E-13  axis 2 distortion coefficient of U2.V2
cal:gnd:distort_bp_3_0     1     BP_3_0     r        6.293886E-11  axis 2 distortion coefficient of U3
cal:gnd:distort_bp_3_1     1     BP_3_1     r       -7.164364E-13  axis 2 distortion coefficient of U2.V
cal:gnd:distort_bp_4_0     1     BP_4_0     r       -8.708176E-13  axis 2 distortion coefficient of U4
\
\ w2
\
cal:gnd:distort_skew       2     SKEW       r        0.000000E+00  [rad] skew component of CD matrix
cal:gnd:distort_a_order    2     A_ORDER    i                   4  polynomial order, axis 1, detector to sky
cal:gnd:distort_a_0_0      2     A_0_0      r        7.597772E-01  axis 1 distortion coefficient of v0
cal:gnd:distort_a_0_1      2     A_0_1      r       -1.192789E-04  axis 1 distortion coefficient of v1
cal:gnd:distort_a_1_0      2     A_1_0      r       -5.040463E-04  axis 1 distortion coefficient of u1
cal:gnd:distort_a_0_2      2     A_0_2      r       -8.064834E-06  axis 1 distortion coefficient of v2
cal:gnd:distort_a_0_3      2     A_0_3      r       -4.935791E-10  axis 1 distortion coefficient of v3
cal:gnd:distort_a_0_4      2     A_0_4      r       -1.303108E-13  axis 1 distortion coefficient of v4
cal:gnd:distort_a_1_1      2     A_1_1      r        1.082862E-06  axis 1 distortion coefficient of u.v
cal:gnd:distort_a_1_2      2     A_1_2      r        3.389170E-10  axis 1 distortion coefficient of u.v2
cal:gnd:distort_a_1_3      2     A_1_3      r       -5.769507E-13  axis 1 distortion coefficient of u.v3
cal:gnd:distort_a_2_0      2     A_2_0      r       -1.349460E-06  axis 1 distortion coefficient of u2
cal:gnd:distort_a_2_1      2     A_2_1      r       -1.297961E-09  axis 1 distortion coefficient of u2.v
cal:gnd:distort_a_2_2      2     A_2_2      r        2.075723E-12  axis 1 distortion coefficient of u2.v2
cal:gnd:distort_a_3_0      2     A_3_0      r        2.959435E-09  axis 1 distortion coefficient of u3
cal:gnd:distort_a_3_1      2     A_3_1      r       -6.743610E-13  axis 1 distortion coefficient of u2.v
cal:gnd:distort_a_4_0      2     A_4_0      r        1.787756E-12  axis 1 distortion coefficient of u4
cal:gnd:distort_a_dmax     2     A_DMAX     r               2.083  [pixel] axis 1 maximum correction
cal:gnd:distort_b_order    2     B_ORDER    i                   4  polynomial order, axis 2, detector to sky
cal:gnd:distort_b_0_0      2     B_0_0      r       -9.433609E-02  axis 2 distortion coefficient of v0
cal:gnd:distort_b_0_1      2     B_0_1      r        5.505028E-04  axis 2 distortion coefficient of v1
cal:gnd:distort_b_1_0      2     B_1_0      r       -2.026974E-04  axis 2 distortion coefficient of u1
cal:gnd:distort_b_0_2      2     B_0_2      r        1.091415E-06  axis 2 distortion coefficient of v2
cal:gnd:distort_b_0_3      2     B_0_3      r       -3.840921E-09  axis 2 distortion coefficient of v3
cal:gnd:distort_b_0_4      2     B_0_4      r       -5.181754E-13  axis 2 distortion coefficient of v4
cal:gnd:distort_b_1_1      2     B_1_1      r       -3.953933E-06  axis 2 distortion coefficient of u.v
cal:gnd:distort_b_1_2      2     B_1_2      r       -9.316313E-10  axis 2 distortion coefficient of u.v2
cal:gnd:distort_b_1_3      2     B_1_3      r        8.534495E-13  axis 2 distortion coefficient of u.v3
cal:gnd:distort_b_2_0      2     B_2_0      r        8.038015E-08  axis 2 distortion coefficient of u2
cal:gnd:distort_b_2_1      2     B_2_1      r        4.101600E-10  axis 2 distortion coefficient of u2.v
cal:gnd:distort_b_2_2      2     B_2_2      r       -5.705721E-13  axis 2 distortion coefficient of u2.v2
cal:gnd:distort_b_3_0      2     B_3_0      r        1.067827E-10  axis 2 distortion coefficient of u3
cal:gnd:distort_b_3_1      2     B_3_1      r        1.952342E-12  axis 2 distortion coefficient of u2.v
cal:gnd:distort_b_4_0      2     B_4_0      r       -1.788157E-13  axis 2 distortion coefficient of u4
cal:gnd:distort_b_dmax     2     B_DMAX     r               1.089  [pixel] axis 2 maximum correction
cal:gnd:distort_ap_order   2     AP_ORDER   i                   4  polynomial order, axis 1, sky to detector
cal:gnd:distort_ap_0_0     2     AP_0_0     r       -7.601833E-01  axis 1 distortion coefficient of V0
cal:gnd:distort_ap_0_1     2     AP_0_1     r        1.214455E-04  axis 1 distortion coefficient of V1
cal:gnd:distort_ap_1_0     2     AP_1_0     r        5.022762E-04  axis 1 distortion coefficient of U1
cal:gnd:distort_ap_0_2     2     AP_0_2     r        8.060749E-06  axis 1 distortion coefficient of V2
cal:gnd:distort_ap_0_3     2     AP_0_3     r        4.733730E-10  axis 1 distortion coefficient of V3
cal:gnd:distort_ap_0_4     2     AP_0_4     r        1.892303E-13  axis 1 distortion coefficient of V4
cal:gnd:distort_ap_1_1     2     AP_1_1     r       -1.080554E-06  axis 1 distortion coefficient of U.V
cal:gnd:distort_ap_1_2     2     AP_1_2     r       -2.655445E-10  axis 1 distortion coefficient of U.V2
```

```
 cal:gnd:distort_ap_1_3     2     AP_1_3     r        6.091029E-13  axis 1 distortion coefficient of U.V3
 cal:gnd:distort_ap_2_0     2     AP_2_0     r        1.357302E-06  axis 1 distortion coefficient of U2
 cal:gnd:distort_ap_2_1     2     AP_2_1     r        1.285175E-09  axis 1 distortion coefficient of U2.V
 cal:gnd:distort_ap_2_2     2     AP_2_2     r       -2.174012E-12  axis 1 distortion coefficient of U2.V2
 cal:gnd:distort_ap_3_0     2     AP_3_0     r       -2.964908E-09  axis 1 distortion coefficient of U3
 cal:gnd:distort_ap_3_1     2     AP_3_1     r        6.893457E-13  axis 1 distortion coefficient of U2.V
 cal:gnd:distort_ap_4_0     2     AP_4_0     r       -1.795530E-12  axis 1 distortion coefficient of U4
 cal:gnd:distort_bp_order   2     BP_ORDER   i                  4  polynomial order, axis 2, sky to detector
 cal:gnd:distort_bp_0_0     2     BP_0_0     r        9.412452E-02  axis 2 distortion coefficient of V0
 cal:gnd:distort_bp_0_1     2     BP_0_1     r       -5.536797E-04  axis 2 distortion coefficient of V1
 cal:gnd:distort_bp_1_0     2     BP_1_0     r        2.031710E-04  axis 2 distortion coefficient of U1
 cal:gnd:distort_bp_0_2     2     BP_0_2     r       -1.087708E-06  axis 2 distortion coefficient of V2
 cal:gnd:distort_bp_0_3     2     BP_0_3     r        3.865684E-09  axis 2 distortion coefficient of V3
 cal:gnd:distort_bp_0_4     2     BP_0_4     r        5.128681E-13  axis 2 distortion coefficient of V4
 cal:gnd:distort_bp_1_1     2     BP_1_1     r        3.953409E-06  axis 2 distortion coefficient of U.V
 cal:gnd:distort_bp_1_2     2     BP_1_2     r        9.209293E-10  axis 2 distortion coefficient of U.V2
 cal:gnd:distort_bp_1_3     2     BP_1_3     r       -8.239603E-13  axis 2 distortion coefficient of U.V3
 cal:gnd:distort_bp_2_0     2     BP_2_0     r       -7.895137E-08  axis 2 distortion coefficient of U2
 cal:gnd:distort_bp_2_1     2     BP_2_1     r       -3.948197E-10  axis 2 distortion coefficient of U2.V
 cal:gnd:distort_bp_2_2     2     BP_2_2     r        5.843392E-13  axis 2 distortion coefficient of U2.V2
 cal:gnd:distort_bp_3_0     2     BP_3_0     r       -1.087914E-10  axis 2 distortion coefficient of U3
 cal:gnd:distort_bp_3_1     2     BP_3_1     r       -1.963102E-12  axis 2 distortion coefficient of U2.V
 cal:gnd:distort_bp_4_0     2     BP_4_0     r        1.753401E-13  axis 2 distortion coefficient of U4
\
\ w3
\
 cal:gnd:distort_skew       3     SKEW       r        0.000000E+00  [rad] skew component of CD matrix
 cal:gnd:distort_a_order    3     A_ORDER    i                  4  polynomial order, axis 1, detector to sky
 cal:gnd:distort_a_0_0      3     A_0_0      r        7.358456E-01  axis 1 distortion coefficient of v0
 cal:gnd:distort_a_0_1      3     A_0_1      r       -6.410136E-04  axis 1 distortion coefficient of v1
 cal:gnd:distort_a_1_0      3     A_1_0      r       -4.837784E-04  axis 1 distortion coefficient of u1
 cal:gnd:distort_a_0_2      3     A_0_2      r       -8.308111E-06  axis 1 distortion coefficient of v2
 cal:gnd:distort_a_0_3      3     A_0_3      r       -1.625272E-10  axis 1 distortion coefficient of v3
 cal:gnd:distort_a_0_4      3     A_0_4      r        2.677086E-13  axis 1 distortion coefficient of v4
 cal:gnd:distort_a_1_1      3     A_1_1      r        8.952514E-07  axis 1 distortion coefficient of u.v
 cal:gnd:distort_a_1_2      3     A_1_2      r        3.550849E-10  axis 1 distortion coefficient of u.v2
 cal:gnd:distort_a_1_3      3     A_1_3      r       -9.680264E-13  axis 1 distortion coefficient of u.v3
 cal:gnd:distort_a_2_0      3     A_2_0      r       -1.754315E-06  axis 1 distortion coefficient of u2
 cal:gnd:distort_a_2_1      3     A_2_1      r       -9.762929E-10  axis 1 distortion coefficient of u2.v
 cal:gnd:distort_a_2_2      3     A_2_2      r        1.454345E-12  axis 1 distortion coefficient of u2.v2
 cal:gnd:distort_a_3_0      3     A_3_0      r        2.879012E-09  axis 1 distortion coefficient of u3
 cal:gnd:distort_a_3_1      3     A_3_1      r       -3.960689E-12  axis 1 distortion coefficient of u2.v
 cal:gnd:distort_a_4_0      3     A_4_0      r        3.033166E-12  axis 1 distortion coefficient of u4
 cal:gnd:distort_a_dmax     3     A_DMAX     r               2.095  [pixel] axis 1 maximum correction
 cal:gnd:distort_b_order    3     B_ORDER    i                  4  polynomial order, axis 2, detector to sky
 cal:gnd:distort_b_0_0      3     B_0_0      r       -8.389715E-02  axis 2 distortion coefficient of v0
 cal:gnd:distort_b_0_1      3     B_0_1      r        5.030167E-04  axis 2 distortion coefficient of v1
 cal:gnd:distort_b_1_0      3     B_1_0      r       -6.788420E-04  axis 2 distortion coefficient of u1
 cal:gnd:distort_b_0_2      3     B_0_2      r        5.610990E-07  axis 2 distortion coefficient of v2
 cal:gnd:distort_b_0_3      3     B_0_3      r       -3.660396E-09  axis 2 distortion coefficient of v3
 cal:gnd:distort_b_0_4      3     B_0_4      r        1.671433E-14  axis 2 distortion coefficient of v4
 cal:gnd:distort_b_1_1      3     B_1_1      r       -3.515651E-06  axis 2 distortion coefficient of u.v
 cal:gnd:distort_b_1_2      3     B_1_2      r       -2.476911E-10  axis 2 distortion coefficient of u.v2
 cal:gnd:distort_b_1_3      3     B_1_3      r        9.798616E-13  axis 2 distortion coefficient of u.v3
 cal:gnd:distort_b_2_0      3     B_2_0      r        5.414236E-07  axis 2 distortion coefficient of u2
 cal:gnd:distort_b_2_1      3     B_2_1      r        1.285471E-10  axis 2 distortion coefficient of u2.v
 cal:gnd:distort_b_2_2      3     B_2_2      r       -2.083238E-12  axis 2 distortion coefficient of u2.v2
 cal:gnd:distort_b_3_0      3     B_3_0      r        8.619879E-11  axis 2 distortion coefficient of u3
 cal:gnd:distort_b_3_1      3     B_3_1      r        1.482141E-12  axis 2 distortion coefficient of u2.v
 cal:gnd:distort_b_4_0      3     B_4_0      r       -7.304812E-13  axis 2 distortion coefficient of u4
 cal:gnd:distort_b_dmax     3     B_DMAX     r               1.300  [pixel] axis 2 maximum correction
 cal:gnd:distort_ap_order   3     AP_ORDER   i                  4  polynomial order, axis 1, sky to detector
 cal:gnd:distort_ap_0_0     3     AP_0_0     r       -7.361246E-01  axis 1 distortion coefficient of V0
 cal:gnd:distort_ap_0_1     3     AP_0_1     r        6.419018E-04  axis 1 distortion coefficient of V1
 cal:gnd:distort_ap_1_0     3     AP_1_0     r        4.828724E-04  axis 1 distortion coefficient of U1
 cal:gnd:distort_ap_0_2     3     AP_0_2     r        8.303367E-06  axis 1 distortion coefficient of V2
 cal:gnd:distort_ap_0_3     3     AP_0_3     r        1.574646E-10  axis 1 distortion coefficient of V3
 cal:gnd:distort_ap_0_4     3     AP_0_4     r       -2.102217E-13  axis 1 distortion coefficient of V4
 cal:gnd:distort_ap_1_1     3     AP_1_1     r       -8.797586E-07  axis 1 distortion coefficient of U.V
 cal:gnd:distort_ap_1_2     3     AP_1_2     r       -2.883046E-10  axis 1 distortion coefficient of U.V2
 cal:gnd:distort_ap_1_3     3     AP_1_3     r        9.855525E-13  axis 1 distortion coefficient of U.V3
 cal:gnd:distort_ap_2_0     3     AP_2_0     r        1.760895E-06  axis 1 distortion coefficient of U2
 cal:gnd:distort_ap_2_1     3     AP_2_1     r        9.707856E-10  axis 1 distortion coefficient of U2.V
 cal:gnd:distort_ap_2_2     3     AP_2_2     r       -1.524870E-12  axis 1 distortion coefficient of U2.V2
 cal:gnd:distort_ap_3_0     3     AP_3_0     r       -2.889421E-09  axis 1 distortion coefficient of U3
 cal:gnd:distort_ap_3_1     3     AP_3_1     r        3.947562E-12  axis 1 distortion coefficient of U2.V
 cal:gnd:distort_ap_4_0     3     AP_4_0     r       -3.042306E-12  axis 1 distortion coefficient of U4
 cal:gnd:distort_bp_order   3     BP_ORDER   i                  4  polynomial order, axis 2, sky to detector
 cal:gnd:distort_bp_0_0     3     BP_0_0     r        8.332980E-02  axis 2 distortion coefficient of V0
 cal:gnd:distort_bp_0_1     3     BP_0_1     r       -5.046199E-04  axis 2 distortion coefficient of V1
 cal:gnd:distort_bp_1_0     3     BP_1_0     r        6.793719E-04  axis 2 distortion coefficient of U1
 cal:gnd:distort_bp_0_2     3     BP_0_2     r       -5.522436E-07  axis 2 distortion coefficient of V2
 cal:gnd:distort_bp_0_3     3     BP_0_3     r        3.670489E-09  axis 2 distortion coefficient of V3
 cal:gnd:distort_bp_0_4     3     BP_0_4     r       -2.075438E-14  axis 2 distortion coefficient of V4
 cal:gnd:distort_bp_1_1     3     BP_1_1     r        3.513457E-06  axis 2 distortion coefficient of U.V
```

```
cal:gnd:distort_bp_1_2     3     BP_1_2     r        2.489261E-10  axis 2 distortion coefficient of U.V2
cal:gnd:distort_bp_1_3     3     BP_1_3     r       -9.405921E-13  axis 2 distortion coefficient of U.V3
cal:gnd:distort_bp_2_0     3     BP_2_0     r       -5.369960E-07  axis 2 distortion coefficient of U2
cal:gnd:distort_bp_2_1     3     BP_2_1     r       -1.178523E-10  axis 2 distortion coefficient of U2.V
cal:gnd:distort_bp_2_2     3     BP_2_2     r        2.077496E-12  axis 2 distortion coefficient of U2.V2
cal:gnd:distort_bp_3_0     3     BP_3_0     r       -8.895805E-11  axis 2 distortion coefficient of U3
cal:gnd:distort_bp_3_1     3     BP_3_1     r       -1.490019E-12  axis 2 distortion coefficient of U2.V
cal:gnd:distort_bp_4_0     3     BP_4_0     r        7.251477E-13  axis 2 distortion coefficient of U4
\
\ w4
\
cal:gnd:distort_skew       4     SKEW       r        0.000000E+00  [rad] skew component of CD matrix
cal:gnd:distort_a_order    4     A_ORDER    i                   4  polynomial order, axis 1, detector to sky
cal:gnd:distort_a_0_0      4     A_0_0      r        4.454888E-01  axis 1 distortion coefficient of v0
cal:gnd:distort_a_0_1      4     A_0_1      r        1.798126E-04  axis 1 distortion coefficient of v1
cal:gnd:distort_a_1_0      4     A_1_0      r       -6.246135E-04  axis 1 distortion coefficient of u1
cal:gnd:distort_a_0_2      4     A_0_2      r       -1.719398E-05  axis 1 distortion coefficient of v2
cal:gnd:distort_a_0_3      4     A_0_3      r        3.413039E-10  axis 1 distortion coefficient of v3
cal:gnd:distort_a_0_4      4     A_0_4      r        3.375647E-12  axis 1 distortion coefficient of v4
cal:gnd:distort_a_1_1      4     A_1_1      r        1.123638E-06  axis 1 distortion coefficient of u.v
cal:gnd:distort_a_1_2      4     A_1_2      r        3.241247E-09  axis 1 distortion coefficient of u.v2
cal:gnd:distort_a_1_3      4     A_1_3      r       -3.767396E-12  axis 1 distortion coefficient of u.v3
cal:gnd:distort_a_2_0      4     A_2_0      r       -4.103560E-06  axis 1 distortion coefficient of u2
cal:gnd:distort_a_2_1      4     A_2_1      r       -2.036670E-09  axis 1 distortion coefficient of u2.v
cal:gnd:distort_a_2_2      4     A_2_2      r        1.857739E-11  axis 1 distortion coefficient of u2.v2
cal:gnd:distort_a_3_0      4     A_3_0      r        1.242150E-08  axis 1 distortion coefficient of u3
cal:gnd:distort_a_3_1      4     A_3_1      r       -3.249992E-11  axis 1 distortion coefficient of u2.v
cal:gnd:distort_a_4_0      4     A_4_0      r        1.445548E-11  axis 1 distortion coefficient of u4
cal:gnd:distort_a_dmax     4     A_DMAX     r               0.971  [pixel] axis 1 maximum correction
cal:gnd:distort_b_order    4     B_ORDER    i                   4  polynomial order, axis 2, detector to sky
cal:gnd:distort_b_0_0      4     B_0_0      r       -5.775286E-02  axis 2 distortion coefficient of v0
cal:gnd:distort_b_0_1      4     B_0_1      r        5.474906E-04  axis 2 distortion coefficient of v1
cal:gnd:distort_b_1_0      4     B_1_0      r       -1.431559E-04  axis 2 distortion coefficient of u1
cal:gnd:distort_b_0_2      4     B_0_2      r        1.364385E-06  axis 2 distortion coefficient of v2
cal:gnd:distort_b_0_3      4     B_0_3      r       -1.534179E-08  axis 2 distortion coefficient of v3
cal:gnd:distort_b_0_4      4     B_0_4      r       -1.931603E-12  axis 2 distortion coefficient of v4
cal:gnd:distort_b_1_1      4     B_1_1      r       -7.968204E-06  axis 2 distortion coefficient of u.v
cal:gnd:distort_b_1_2      4     B_1_2      r       -9.571209E-10  axis 2 distortion coefficient of u.v2
cal:gnd:distort_b_1_3      4     B_1_3      r        5.169349E-12  axis 2 distortion coefficient of u.v3
cal:gnd:distort_b_2_0      4     B_2_0      r        1.315098E-06  axis 2 distortion coefficient of u2
cal:gnd:distort_b_2_1      4     B_2_1      r        9.606579E-10  axis 2 distortion coefficient of u2.v
cal:gnd:distort_b_2_2      4     B_2_2      r       -1.052149E-11  axis 2 distortion coefficient of u2.v2
cal:gnd:distort_b_3_0      4     B_3_0      r       -5.358762E-10  axis 2 distortion coefficient of u3
cal:gnd:distort_b_3_1      4     B_3_1      r        1.290359E-11  axis 2 distortion coefficient of u2.v
cal:gnd:distort_b_4_0      4     B_4_0      r       -1.173857E-11  axis 2 distortion coefficient of u4
cal:gnd:distort_b_dmax     4     B_DMAX     r               0.582  [pixel] axis 2 maximum correction
cal:gnd:distort_ap_order   4     AP_ORDER   i                   4  polynomial order, axis 1, sky to detector
cal:gnd:distort_ap_0_0     4     AP_0_0     r       -4.457576E-01  axis 1 distortion coefficient of V0
cal:gnd:distort_ap_0_1     4     AP_0_1     r       -1.781952E-04  axis 1 distortion coefficient of V1
cal:gnd:distort_ap_1_0     4     AP_1_0     r        6.204521E-04  axis 1 distortion coefficient of U1
cal:gnd:distort_ap_0_2     4     AP_0_2     r        1.719030E-05  axis 1 distortion coefficient of V2
cal:gnd:distort_ap_0_3     4     AP_0_3     r       -3.781631E-10  axis 1 distortion coefficient of V3
cal:gnd:distort_ap_0_4     4     AP_0_4     r       -2.994271E-12  axis 1 distortion coefficient of V4
cal:gnd:distort_ap_1_1     4     AP_1_1     r       -1.123275E-06  axis 1 distortion coefficient of U.V
cal:gnd:distort_ap_1_2     4     AP_1_2     r       -2.907111E-09  axis 1 distortion coefficient of U.V2
cal:gnd:distort_ap_1_3     4     AP_1_3     r        3.797752E-12  axis 1 distortion coefficient of U.V3
cal:gnd:distort_ap_2_0     4     AP_2_0     r        4.123874E-06  axis 1 distortion coefficient of U2
cal:gnd:distort_ap_2_1     4     AP_2_1     r        2.033637E-09  axis 1 distortion coefficient of U2.V
cal:gnd:distort_ap_2_2     4     AP_2_2     r       -1.931343E-11  axis 1 distortion coefficient of U2.V2
cal:gnd:distort_ap_3_0     4     AP_3_0     r       -1.266208E-08  axis 1 distortion coefficient of U3
cal:gnd:distort_ap_3_1     4     AP_3_1     r        3.258225E-11  axis 1 distortion coefficient of U2.V
cal:gnd:distort_ap_4_0     4     AP_4_0     r       -1.463342E-11  axis 1 distortion coefficient of U4
cal:gnd:distort_bp_order   4     BP_ORDER   i                   4  polynomial order, axis 2, sky to detector
cal:gnd:distort_bp_0_0     4     BP_0_0     r        5.767048E-02  axis 2 distortion coefficient of V0
cal:gnd:distort_bp_0_1     4     BP_0_1     r       -5.516974E-04  axis 2 distortion coefficient of V1
cal:gnd:distort_bp_1_0     4     BP_1_0     r        1.440997E-04  axis 2 distortion coefficient of U1
cal:gnd:distort_bp_0_2     4     BP_0_2     r       -1.363994E-06  axis 2 distortion coefficient of V2
cal:gnd:distort_bp_0_3     4     BP_0_3     r        1.517287E-08  axis 2 distortion coefficient of V3
cal:gnd:distort_bp_0_4     4     BP_0_4     r        1.958353E-12  axis 2 distortion coefficient of V4
cal:gnd:distort_bp_1_1     4     BP_1_1     r        7.959111E-06  axis 2 distortion coefficient of U.V
cal:gnd:distort_bp_1_2     4     BP_1_2     r        9.315308E-10  axis 2 distortion coefficient of U.V2
cal:gnd:distort_bp_1_3     4     BP_1_3     r       -4.678544E-12  axis 2 distortion coefficient of U.V3
cal:gnd:distort_bp_2_0     4     BP_2_0     r       -1.314523E-06  axis 2 distortion coefficient of U2
cal:gnd:distort_bp_2_1     4     BP_2_1     r       -8.924626E-10  axis 2 distortion coefficient of U2.V
cal:gnd:distort_bp_2_2     4     BP_2_2     r        1.061448E-11  axis 2 distortion coefficient of U2.V2
cal:gnd:distort_bp_3_0     4     BP_3_0     r        5.235808E-10  axis 2 distortion coefficient of U3
cal:gnd:distort_bp_3_1     4     BP_3_1     r       -1.295506E-11  axis 2 distortion coefficient of U2.V
cal:gnd:distort_bp_4_0     4     BP_4_0     r        1.174041E-11  axis 2 distortion coefficient of U4
```

Appendix C: Investigation Into Time Variation of Distortion

After the IOC period, production processing of survey data began. This employed the distortion models obtained from IOC and also an expanded partitioning of the PSFs used for point-source extraction from 5×5 to 9×9 in W1 and W2. Accordingly, the partitioning used for binned residuals in distortion fitting was changed from 31×31 to 45×45 in order to be commensurable with the 5×5 PSF partitions.

When symptoms of cryogen depletion began to appear in August 2010, distortion calibrations were run to check stability, and it was observed that W3 and W4 showed significant differences from the IOC models. Tracking those changes will be a separate activity, but one product of those studies was a set of models computed for the period just before cryogen depletion became noticeable. The differences between these and the IOC models were small enough not to threaten astrometric accuracy requirements but large enough to be potentially significant statistically. In any case, it had been planned to recalibrate distortion for the final processing based on a much larger data sample than IOC could provide, and so it was decided to set up the data for this in several sets of chronologically contiguous periods which could be used to check for time variability.

Five periods were selected for this analysis, each of 5-day duration, and centered on MJD 212.5, 262.5, 312.5, 362.5, and 412.5. This 200-day span was originally intended to be filled completely with 5-day data sets, but given the extreme computational load required to perform such exhaustive calibrations and the lack of need for it found subsequently, the analysis was performed with those five periods alone.

Models for W1-W4 were computed for each of the five periods and also for the combined 25-day data set. Given that the differences between the earliest and latest models were about the same as the residuals in the 25-day models, and given that these residuals are much too small to threaten any mission requirements, the latter models are intended for use in the final data processing. Furthermore, as noted earlier, the fitting residuals are slightly overestimated because of the fact that the gnDSTR program outputs residuals relative to the first-pass fit, and excluding samples with residuals above threshold causes the second-pass fit to yield a better model with smaller residuals. In the end, the clear visibility of the 9×9 PSF partitions in the residual images for W1 and W2 argues strongly that the residuals are dominated by very small systematic point-source extraction errors with spatial structure that cannot be removed with any polynomial of reasonable order.

This argument is strengthened by the observation that the residuals in the 5-day periods are essentially the same as those in the 25-day period, indicating the same underlying systematic limitation. If there were a significant time variation of a long-term drift variety, it would be expected to inflate the residuals of the 25-day period relative to those of the 5-day periods, and that is not seen. Table C-1 below shows the W1 residuals for the 25-day period and the two endpoint periods, JD212.5 and JD412.5.

Period/Axis	Mean	Sigma	Min	Max	Median	1%-tile	99%-tile
25-Day/X	0.00016	0.03644	-0.08390	0.09606	-0.00066	-0.06650	0.08068
JD212.5/X	0.00245	0.03778	-0.09498	0.10607	0.00102	-0.07175	0.08426
JD412.5/X	-0.00256	0.03630	-0.09234	0.09361	-0.00368	-0.07417	0.07788
25-Day/Y	0.00060	0.01559	-0.05461	0.08401	0.00003	-0.03432	0.04386
JD212.5/Y	-0.00393	0.01653	-0.05701	0.09080	-0.00429	-0.03883	0.04397
JD412.5/Y	0.00544	0.01675	-0.04477	0.07794	0.00426	-0.03108	0.04950

Table C-1. W1 Residuals for 25-Day Period and JD212.5 & JD412.5 Periods (arcsec)

The spatial distribution of the residuals over the arrays is shown below for the 25-day models, along with the minimum and maximum values in arcsec units.

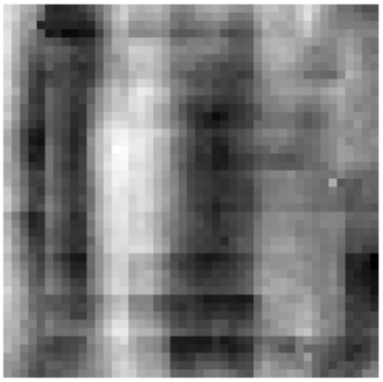

W1 X (-0.0939 to +0.0961)

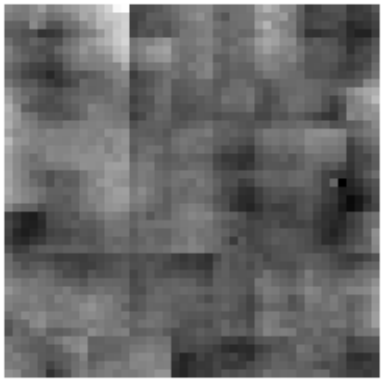

W1 Y (-0.0546 to +0.0840)

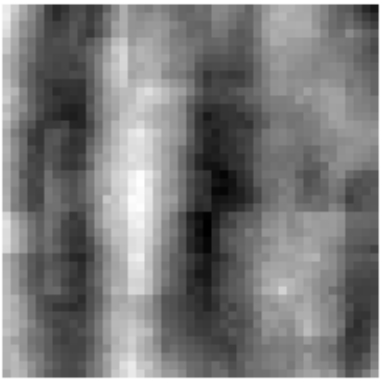

W2 X (-0.0828 to +0.1006)

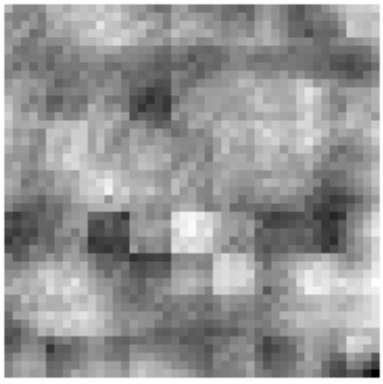

W2 Y (-0.0481 to +0.0377)

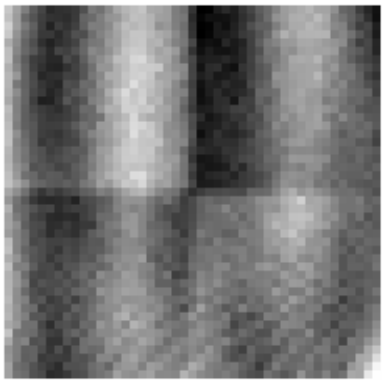

W3 X (-0.1081 to +0.1108)

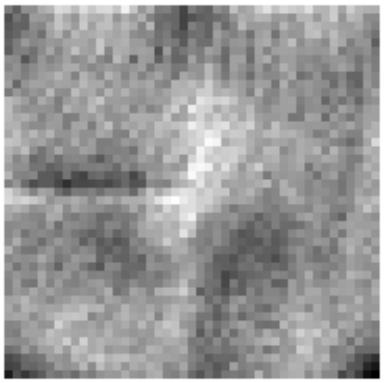

W3 Y (-0.0624 to +0.0836)

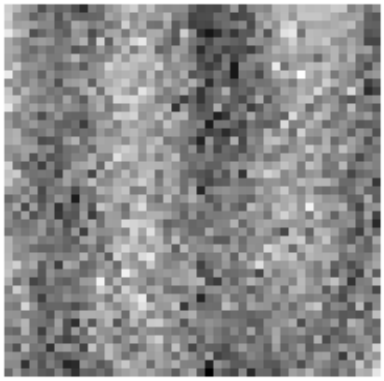

W4 X (-0.1551 to +0.2321)

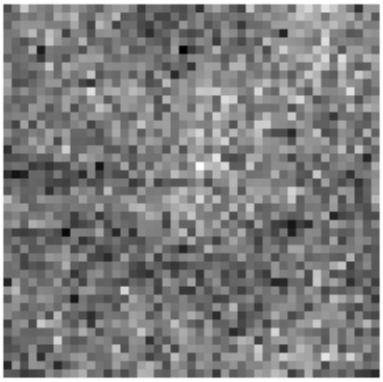

W4 Y (-0.1106 to +0.2712)

References

J. Fowler, H. McCallon, **gnDSTR SDS**, WSDC D-D013.

J. Fowler, H. McCallon, **PRex SDS**, WSDC D-D003.

F. Masci, F. McCallon, J. Fowler, "Distortion Calibration and Code-V Modelling", http://wise2.ipac.caltech.edu/staff/fmasci/codeVdist.html

---